PLASMA RESONANCE IN SOME III-V ALLOYS

by

Hassan Momen Heravi

Thesis submitted to the School of Graduate Studies in partial fulfilment of the requirements of the degree of Master of Science in Physics

Department of Physics
Faculty of Science and Engineering
University of Ottawa
Ottawa, Ontario,

1977.

LIST OF CONTENTS

ACKNOWLEDGEMENTS

I would like to thank sincerely my supervisor, Professor J. C. Woolley, for his kindness and his comments which were of great value throughout the course of this project. I would also like to thank him for his guidance which was indispensable in the preparation of this thesis.

Some of the equipment used for this project was designed and built in co-operation with the electrical and the mechanical work-shops of the Physics Department; for their assistance my special thanks are due to Mr. A. R. Buser and his assistant, Mr. M. G. Ruscher, who built the chopper driver, signal matching impedance and attenuation systems for this project. I would also like to thank all members of the mechanical work-shop especially Mr. C. N. Goodchild who prepared the optical holder for double beam arrangement.

I would also like to acknowledge my indebtedness to the Physics Department for their financial assistance which was provided throughout the course of this project.

ABSTRACT

Measurements of reflectivity and Hall effect have been made on polycrystalline n-type samples of GaAs and alloys of the systems $GaAs_xSb_{1-x}$ and $Ga_{1-x}Al_xAs$ to find values of electron effective mass at the bottom of the conduction band m^*_{oo}/m.

The experimental data were obtained with a Baird monochromator which was modified to give double beam operation and extended wavelength range up to 30 μm, so that measurements of the free carrier reflectivity could be made on samples with low carrier concentration. The reflection coefficient R and hence the index of refraction n were obtained from the experimental measurements. The variation of n^2 was plotted as a function of the square of the wavelength. For each sample, the graphical result (n^2 vs λ^2) was found to be a straight line and it was extrapolated to zero wavelength to obtain the optical dielectric constant ε_∞. The slope of the line also was determined and used to obtain the value of effective mass at the bottom of the conduction band. For the systems $GaAs_xSb_{1-x}$ the alloy compositions were determined by the X-ray powder photograph method.

For the two alloy systems $GaAs_xSb_{1-x}$ and $Ga_{1-x}Al_xAs$, optical dielectric constant and effective mass values were measured from infrared reflectivity for the first time. The values of the effective masses were determined by the simultaneous solution of the integrals giving the statistical carrier concentration and the slope of the free carrier reflectivity under the condition of the general degeneracy, the lattice

contribution to the slope being taken into account.

Theoretical values of the effective masses in the (000) conduction band as a function of alloy composition were calculated for the alloy system $GaAs_xSb_{1-x}$ using the disorder equation (73W) and Kane equation (57K) for the effective masses. The experimental results were found to be in better agreement with the disorder equation of the effective mass than with the Kane equation.

Finally, to complete the outline of the project, it should be mentioned that the values of optical Fermi energy, dielectric constant, optical relaxation time, optical mobility and optical conductivity were calculated for 12 samples of the alloys $GaAs_xSb_{1-x}$ and $Ga_{1-x}Al_xAs$.

LIST OF TABLES

LIST OF FIGURES

I-1 INTRODUCTION

Historically, the fundamental phenomenon in semiconductors was underlined by Faraday (F1) in 1833 by his discovering the negative temperature coefficient of resistivity of silver sulphide. Subsequently, rectification at a contact between a metal and a semiconductor was discovered by F. Braun in 1874, and used in the early stage of the development of the point-contact crystal in radio engineering. In 1874, the photo-conductivity effect was pointed out by Smith. In 1879 (H1), the phenomenon which is now known as the Hall effect was found and this later proved to be extremely helpful in bettering the understanding of conduction processes in semiconductors.

In 1928, Langmuir (28L) introduced plasma oscillation, as the longitudinal oscillation of electron gas which is analogous to sound waves. In 1949, the first publication by Bardeen and Brattain (B2) on the transistor effect (semiconductor triode) had a great impact on technology. Consequently intensive research has been carried out on the properties of materials giving transistor effect, i.e., germanium and silicon. Later, in 1952, Welker (52W) demonstrated that semiconducting properties were present also in many of the III-V, II-VI and I-VII compounds and their alloys. The study of the properties of III-V compounds and their alloys has become increasingly important in modern technology because of such applications as photo-detectors, light generators, thermoelectric generators, Gunn oscillators and integrated optical communication systems. These possible applications of semiconductors in technology created a good atmosphere for the investigation of parameters related to the band

structure (e.g. effective mass and energy gap) of those material which may be used in new applications.

The theory relating to optical effective mass and plasma resonance in a conductor was developed in a series of papers by Bohm and Dines (51B, 53B, 55B). The relationship between the theoretical expression and the results of experimental measurements of optical effective mass of free carrier in a semiconductor were developed by Fan and Spitzer (57F). The form of this analysis together with later developments will be discussed in the following section.

I-2 BAND THEORY

Band theory is a method of investigating the states and energies of electrons assumed to be nearly free in a periodic potential. The experimental and theoretical results show that the allowed energies lie in bands separated by gaps of forbidden energies. The theoretical analysis of the band structure involves solution of the wave equation for the multi-particle case and various methods of approximation have been proposed and used. Usually, the solutions are guided by the use of group theory to impose the effects of the symmetry properties of the solid concerned. In almost all cases, the analyses need the use of experimental measurements to provide values of adjustable parameters, and the measurement of optical, electrical and magnetic properties amongst others have been found very important in the development of band structure analysis.

In the non-relativistic calculations of band structures, assuming

the ions are at rest and considering a single electron moving in the periodic field of the lattice, the action of the other electrons on the electron under study can be replaced by a periodic potential with the periodicity of the lattice. In the case of the collective motion of the electrons in plasma resonance, (the subject studied in this work) the electrons are regarded as a collection of particles, occupying one-electron states in accordance with the rules of Fermi-Dirac statistics.

For a periodic potential, the non-relativistic Schrodinger equation is

$$\frac{\hbar^2}{2m} \nabla^2\psi + \{E - V(r)\}\psi = 0 \qquad \text{(I-1)}$$

satisfied by the Bloch function $\psi(x) = \exp(ik.r)\, U(r)$ where $U(r)$ has the periodicity of the lattice. For each particular value of k_i, $i = 1,n$ there are an infinite number of solutions. The resulting energy distribution is simply illustrated by considering the one-dimensional case. For a quasi-continuous variation of k, the resulting energy values lie on curves which show discontinuities at values of k given by

$$k = \pm \frac{n\pi}{a} \qquad \text{(I-2)}$$

where n is integral and a is the periodicity of the one-dimensional array. Thus the energy spectrum is divided into allowed and forbidden bands. When this analysis is made in the three-dimensional case, it is found that for electron velocities in every direction in normal space, discontinuities in energy occur at certain k values in the corresponding direction in k-space. The surface in k-space defined by the first discontinuity in energy has a particular shape and is called the first Brillouin boundary and the enclosed volume is the first Brillouin zone. It contains all allowed state up to the first discontinuity and each point satisfies the restric-

tions imposed by equation (I-2) in three dimension, corresponding to a quantum state. Figure (I-1) shows the first Brillouin zone of the face centered cubic lattice, with the symmetry points and axes. The range of energy obtained by taking all possible values of k within one zone constitutes one energy band. Within each Brillouin zone, surfaces of constant energy can be drawn. In semiconductor work, these are mainly of interest close to the energy minimum of almost empty (conduction) bands or to the energy maximum of almost filled (valence) bands and in these ranges the constant energy surfaces usually have relatively simple form. In the present work we are concerned only with the conduction band energy surfaces. In all III-V compounds, the conduction band minima occur either at the origin of k space ((000) or Γ point) or along the directions of highest symmetry, i.e. the <100> or <111> directions in k space. Thus the constant energy surfaces of interest are, to a good approximation, either spheres around the Γ point or ellipsoids of revolution with their long axes along the <100> or <111> directions. Hence most band structure diagrams are drawn to show the variation of energy as a function of the value of k from the Γ point to the Brillouin zone boundary in the <111> directions (L point) and the <100> directions (X point).

I-31 Energy Band Structure of GaAs

The band structure of GaAs in the vicinity of the band edge is shown in Figure (I-2). The lowest minimum of the conduction band lies at the centre of the Brillouin zone (Γ), where the value of the conduction

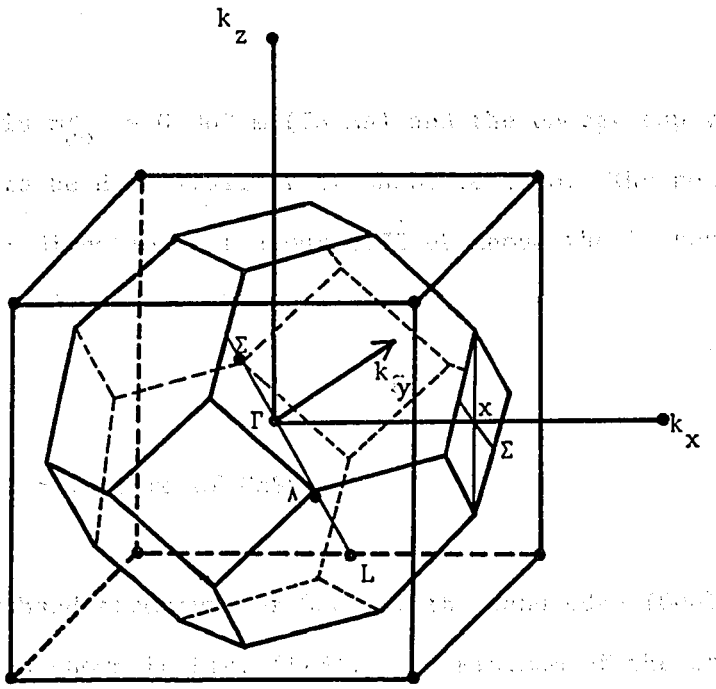

Figure (I-1): First Brillouin zone of the f.c.c. lattice (Ref. 72C)

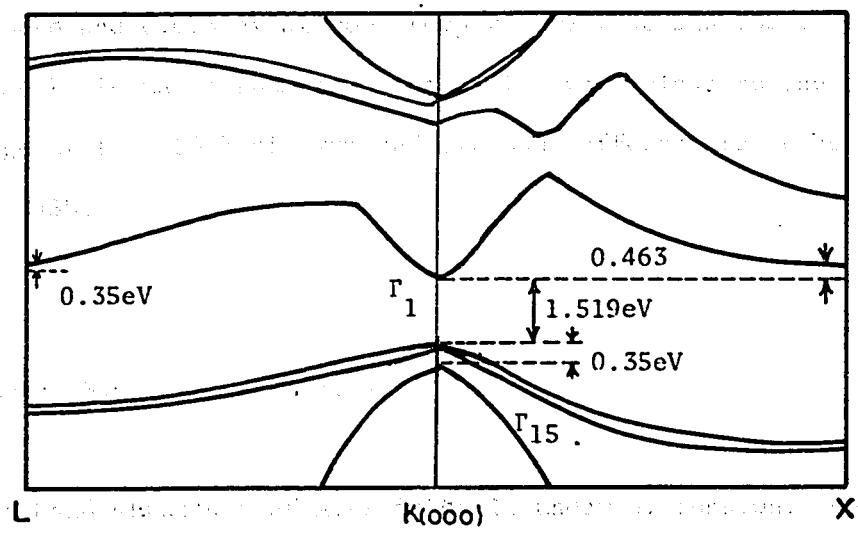

Figure (I-2): The energy band structure of GaAs.

band effective mass is m^*_{oo} = 0.067 m (76 As) and the energy gap value has been determined to be E_o = 1.519 eV at absolute zero. The next minima occur along the <111> directions at about 0.35 eV above the Γ_1 band and have effective mass m*(L) = 0.56 m at absolute zero.

I-32 Energy Band Structure of GaSb

The energy band structure of GaSb at the band edge (000) and in the <111> direction is shown in Fig. (I-3). The minimum of the conduction band lies at the centre of the Brillouin zone (Γ_1) and has effective mass m^*_{oo} = 0.042 m and the energy gap E_o = 0.80 eV at absolute zero. The energy separation, ΔE, between (000) and <111> minima was found to be 0.080 eV at absolute zero and 0.073 eV at room temperature (70C and 73S). This shows that the L minima at room temperature lie very close to the conduction band edge at the (000) minimum and two band effects are to be expected for GaSb.

I-33 Energy Band Structure of AlAs

The band structure of AlAs is still under discussion. Recently, theoretical calculations have been made by Hess et al. (73H) and (69S) using a k.p analysis. They calculated the conduction band effective mass at the Γ point to be m^*_{oo} = 0.15 m. Using this data as a reference point in their calculation, they found the lowest minima for the conduc-

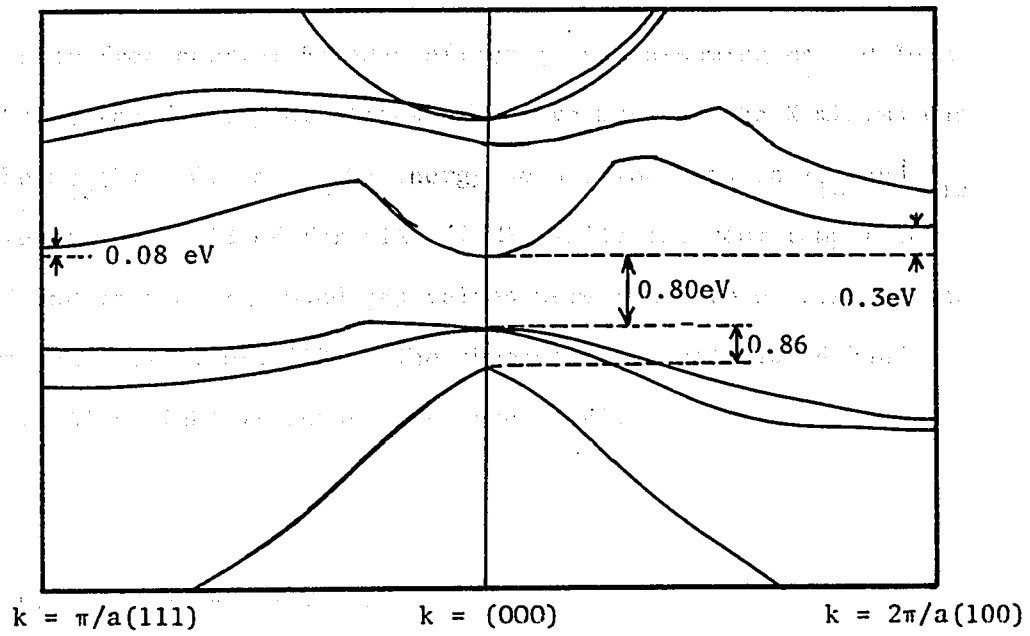

Figure (I-3): The energy band structure of GaSb (70C)

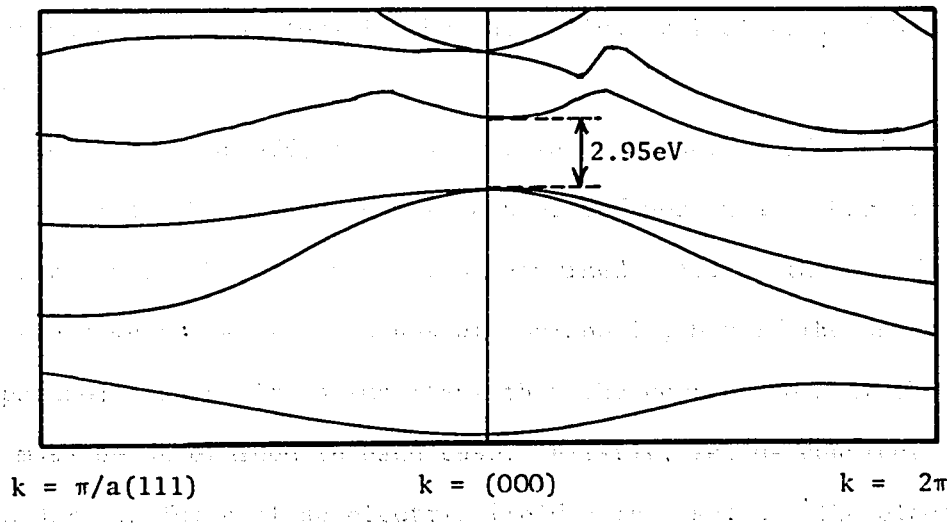

Figure (I-4): The energy band structure of AlAs (73H).

tion band to be the six equivalent minima along the Δ directions near the X points.

From free carrier Faraday effect (71R), assuming $m_c^* = 0.16$ m at the Γ band, the density of states effective mass at the X minima was found to be $m_{lc}^*(X) = 0.5$ m. The energy separation between X_{lc} and Γ_{lc} was reported to be 0.873 eV for AlAs (73M), while the room temperature direct and indirect energy band gap values were found to be 2.95 eV and 2.07 eV respectively (70L, 71R). The theoretically calculated band structure of AlAs (73H) is shown in Figure (I-4).

I-4 CONCEPT OF EFFECTIVE MASS

Much experimental and theoretical research in semiconductors is designed to determine band parameters. This section considers the investigation of the effective mass values, which are used to a considerable extent as known parameters in the theoretical calculation of band structures.

The concept of effective mass arises in a number of analyses (64K, 72Z), so that the effective mass can be defined in a number of ways depending upon which phenomenon is being examined. All of these definitions reduce to the same value if the bands are parabolic, but if the bands do not have parabolic shape it is important that the correct form of the effective mass be determined in each case. Firstly, let us consider an electron under the force of an electric field E in a solid. The electron in such conditions responds in such a way that its wave vector k increases

linearly with time according to the relation

$$\hbar \frac{dk}{dt} = eF$$

The mean velocity of the electron in band n with wave vector k is:

$$v = \frac{1}{\hbar} \nabla_k E_n(k)$$

so that the mean acceleration is

$$\frac{dv}{dt} = \frac{1}{\hbar} \left(\frac{\partial}{\partial t}\right) \nabla_k E_n(k) = \Sigma \frac{1}{\hbar} \frac{\partial v}{\partial k_\beta} \cdot \frac{\partial k_\beta}{\partial t}$$

or

$$\frac{\partial v}{\partial t} = \frac{1}{\hbar^2} \Sigma \frac{\partial^2 E_n(k)}{\partial k_\alpha \partial k_\beta} eE_\beta = \Sigma \left(\frac{1}{m_n}\right)_{\alpha\beta} eE_\beta$$

As is shown in this equation and found by experiment, the effective mass may be quite different in different directions if the constant energy surfaces are not spherical. Physically, this means that the same electric field applied in different directions will cause different accelerations. Thus, formally, the mass has been replaced by a tensor (effective mass tensor) with components

$$\left(\frac{1}{m_n}\right) = \frac{1}{\hbar^2} \left(\frac{\partial^2 E_n(k)}{\partial k_\alpha \partial k_\beta}\right)$$

Let us call this definition of effective mass, band curvature effective mass. When the non-diagonal terms of the effective mass tensor vanish, the energy is a function of k_x, k_y, k_z only. One important case is $E = \text{const}\ (k_x^2 + k_y^2 + k_z^2)$ and in this case m* simplifies to a scalar.

$$\left(\frac{1}{m^*}\right) = \frac{1}{\hbar^2} \left(\frac{\partial^2 E}{\partial k^2}\right) \qquad \text{(I-4)}$$

In the isotropic case, m* is thus inversely proportional to the curvature

of the E-k curve at the given point and m* is positive if the curvature is convex towards the k-axis and is negative if the curvature is concave.

I-41 Cyclotron Effective Mass

Under the influence of a strong magnetic field, electrons move in orbits, in such a way that the action of the magnetic field on the electrons under study is given by $\frac{d}{dt}(\hbar k) = ev_{\perp}B$ where $v_{\perp}$ is the velocity of the electron in a plane perpendicular to the magnetic field and can be written in the form

$$v_{\perp} = \frac{1}{h}\frac{dE}{dk_{\perp}}$$

In the presence of the magnetic field, the expression for the Lorentz force on an electron is evB, so that the time required for the momentum to change by dP in the plane perpendicular to the magnetic field is dP/evB. The time required to complete a revolution is

$$T = \frac{1}{eB}\frac{dP}{v} = \frac{1}{eB}\int \frac{dPdP_{\perp}}{dE} = \frac{2\pi}{\omega_c} = \frac{2\pi m_c^*}{eB} \qquad \text{(I-5)}$$

where $\omega_c = \frac{eB}{m_c^*}$ is called the cyclotron frequency, and m_c^* is the cyclotron effective mass. Therefore the cyclotron effective mass for an orbit can be defined by

$$m_c^* = \frac{1}{2\pi}\int \frac{dPdP_{\perp}}{dE} \qquad \text{(I-6)}$$

where the integration is carried out along the curve bounding a cross-

section of a surface of the orbit in momentum space and has a value equal to the area dR(P) of the cross-section

$$m_c^* = \frac{1}{2\pi} \frac{dR(P)}{dE}$$

For a spherical constant energy surface R(P) reduces to $R(P) = \pi P^2 = \pi\hbar^2 k^2$ Therefore we can define the general expression for cyclotron effective mass for a spherical constant energy surface as

$$\frac{1}{m_c^*} = \frac{1}{\hbar^2 k} \frac{dE}{dk} \qquad \text{(I-7)}$$

Cyclotron resonance experiments are widely used to better the understanding of the energy band structure in semiconductors, since they enable one to measure directly the effective mass of holes and electrons. The results give explicit information about energy surfaces at the top of the valence band and at the bottom of the conduction band, since the experimental value of the cyclotron effective mass can be interpreted as the slope of the constant energy surface in k space (E vs. k). It can be shown that the effective mass measured in magneto-optic phenomena and plasma reflectivity is the cyclotron effective mass. Cyclotron resonance of free carriers in semiconductors has usually been measured at microwave frequencies (60L) in high magnetic fields and low temperatures.

I-42 Faraday Rotation Effective Mass

This effective mass is measured by the rotation of the plane of linear polarization due to the difference of refractive indices for left

and right circularly polarized components. For strong degeneracy conditions with spherical constant energy surfaces, the Faraday rotation is given by

$$\theta = \frac{e^3 B \lambda^2}{8\pi\sqrt{\epsilon}\, c^4} \cdot \frac{N}{m^{*2}} \qquad \text{(I-8)}$$

where θ is the Faraday angle and is inversely proportional to the square of the effective mass, which allows a direct measurement of the effective mass value if the electron concentration N is known. The effect of an external magnetic field on the band structure of a solid may be interpreted in terms of Landau levels. When the magnetic field is applied to an n-type semiconductor, the energy of the lowest level of the conduction band increases due to the formation of the Landau levels, the change being dependent on the magnitude of the magnetic field. Thus as the field is increased, the lower energy levels are gradually forced through the Fermi energy. The effective mass measured when the lowest energy is at the Fermi level due to the change in the distribution of the energy band (due to the applied magnetic field) is called the effective mass at the Fermi level, and for spherical energy surfaces it is expressed by

$$\frac{1}{m^*_f} = \frac{1}{\hbar^2 k} \left(\frac{\partial E}{\partial k}\right)_f \qquad \text{(I-9)}$$

where the right hand side is evaluated at the Fermi level f. In the case of a multi-ellipsoid band with cubic symmetry, the effective mass m* is a combination of the longitudinal and transverse components and can be represented by the quantity

$$m^*_f = \left(\frac{3b}{b+2}\right)^{\frac{1}{2}} m^*_t \quad ; \qquad b = \frac{m_\ell}{m_t} \qquad \text{(I-10)}$$

The Faraday rotation measurement is practically convenient for investigation of the concentration and temperature dependences of the effective mass in semiconductors.

I-43 Conductivity Effective Mass

This effective mass usually applies in transport and optical properties of a solid. For a spherical energy surface the conductivity effective mass will be defined by equation (I-3). In the case of energy surfaces which are ellipsoids of revolution, the effective mass value is expressed by

$$\frac{1}{m^*} = \frac{1}{3}\left(\frac{2}{m_t^*} + \frac{1}{m_\ell^*}\right)$$

where m_ℓ is the value of the effective mass associated with the longitudinal axis of the ellipsoidal energy surface and m_t is that associated with each of the two transverse axes.

When a magnetic field is applied to a solid, if the degeneracy condition is not satisfied or the band is not parabolic, it is difficult to define a special relation for the effective mass value at the bottom of the conduction band. Recently Kukharskii (74K) and Arushanov (75A) reported a method by which it is possible to calculate the value of the conductivity effective mass at the bottom of the conduction band m_{oo}^* as a function of the value of m_c^* obtained from experiment and of the carrier concentration including the condition of degeneracy applying to the sample under investigation. They give their results for spherical constant energy surfaces

with nonparabolic bands. In the case of ellipsoidal constant energy surfaces, their result is reduced to an expression for the density of state effective mass m^*_{od} at the bottom of the band as a function of m^*_d.

I-44 Density of States Effective Mass

The density-of-states effective mass, defined as the effective mass averaged over all the occupied states, is frequently obtained from electrical transport properties of a semiconductor. The combined density of states mass m_d appears in the expression for the electron concentration N as a function of temperature. For a parabolic band at the Fermi level N is expressed by

$$N = \frac{\sqrt{2}(m^*_d \, k_B T)^{3/2}}{\pi^3 \hbar^3} F_{1/2}(f)$$

where $F_{1/2}(f)$ is the Fermi integral. In the case of multi-ellipsoid models with parabolic bands, the density of states effective mass m^*_d is defined by the expression

$$m^*_d = N^{2/3} (m^{*2}_t \, m^*_\ell)^{1/3}$$

The relation between density of state effective mass and effective mass at the bottom of conduction band for nonparabolic band can be found in the literature (74K, 69B).

In addition to the methods listed in the present section, certain other methods have also been used to measure effective mass value. Thus the Nernst-Ettingshausen effect provides one method of determining

effective mass values from thermomagnetic phenomena (62W, 62K). Measurements of magnetic susceptibility (62Z) have also been used to give effective mass values. One other method of determining effective mass values is plasma resonance measurements. This is the method used in the present work and will be discussed in detail in the following chapter.

I-5 TEMPERATURE VARIATION OF ENERGY GAP AND CONDUCTION BAND EFFECTIVE MASS

Two mechanisms are usually considered in determining the change of band gap with temperature, i.e. thermal expansion of the lattice and interaction of the carriers with phonons. As might be expected, the band structure is a function of temperature, so that both the effective mass and the energy gap change as the temperature changes. Furthermore, for a small direct band gap, the relative change in the energy gap is very similar to the relative change in the effective mass (57E). For a sample with sufficiently high carrier concentration, the measurements yield a value of effective mass not near the extremum of the energy band but at the Fermi level and hence the measured effective mass depends less strongly on the energy gap. We might expect the effective mass dependence upon temperature to be determined by the two effects mentioned above. However, Ehrenreich (57E) demonstrated that the interaction with phonons makes a negligibly small contribution to the temperature dependence of the effective mass. Hence, it follows that the whole of the temperature dependence of the effective mass is due only to the thermal expansion of the lattice

while both effects are important in determining the value of band gap. Both effective mass and energy gap show a negative temperature coefficient over the whole temperature range but because of the above effects these coefficients are not similar. At high temperatures, in addition to the above effects, the energy gap can be affected by impurity concentration, as an impurity band may affect the band shape and position (70H, 63A), causing some deviation of the conduction band minimum from its normal position in k-space . However such an effect is beyond the scope of the present work. Furthermore, the effect of temperature changes the distribution of the free carrier from a Fermi to a Boltzamann distribution hence affecting the value of effective mass observed in the measurement.

To give an expression for the variation of effective mass with temperature Ehrenreich (57E) has indicated that the relation giving a reasonable approximation is

$$\frac{m^*_{oo}(T)}{m} = \frac{m^*_{oo}(0)}{m} \quad \frac{E^*_o(T)}{E_o(0)}$$

where $E^*_o(T)$ is the effective mass band gap at temperature T and m^*_{oo}/m is the bottom of the band effective mass ratio. This topic will be discussed further in sections II-2 and V- 2.

I-6 EARLIER WORK ON THE $GaAs_xSb_{1-x}$.

Unlike many of the III-V alloy systems which have been investigated in considerable detail (72R and (75K1), the alloy system $GaAs_xSb_{1-x}$ does not

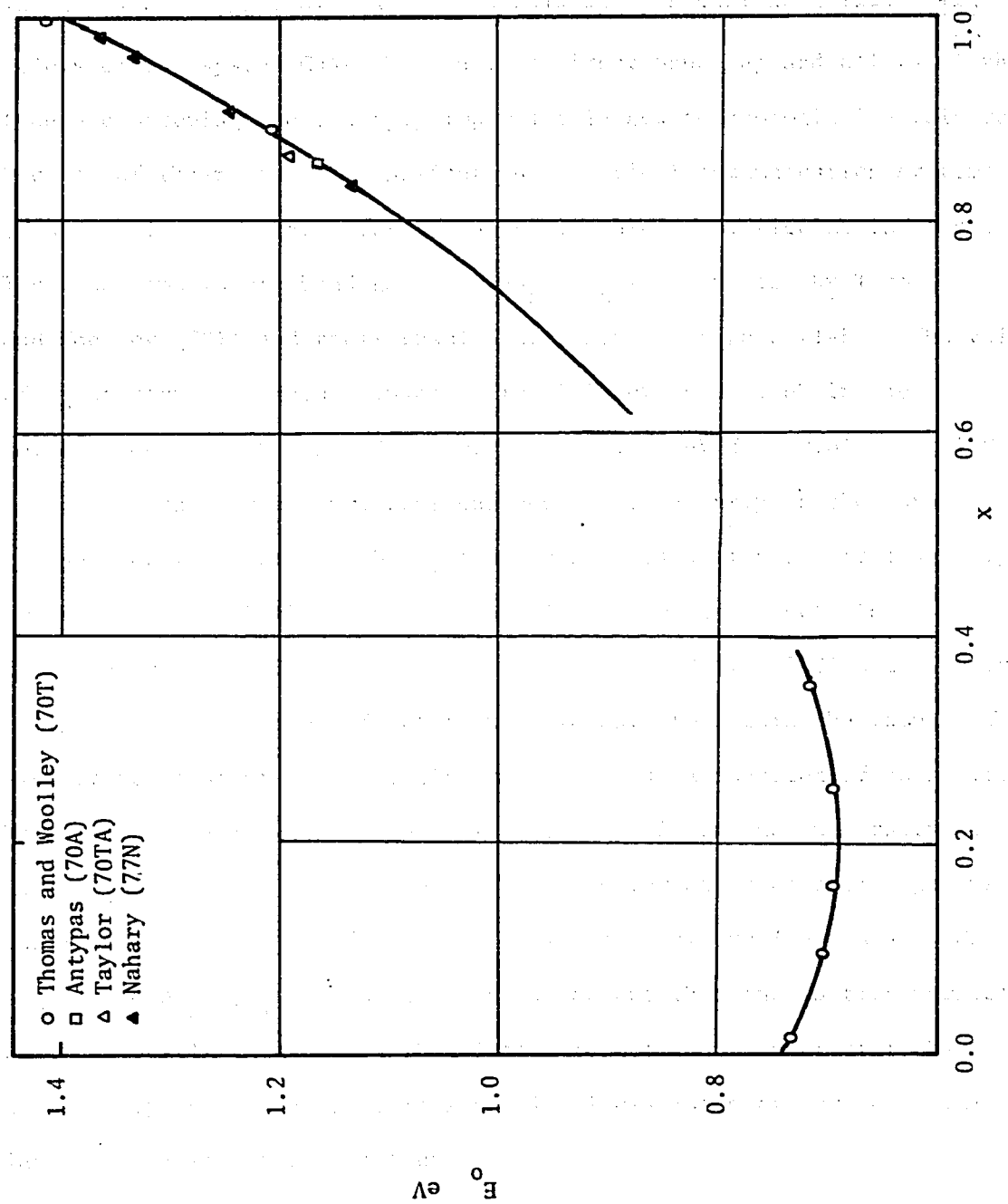

Figure (I- 5): Values of energy gap as a function of composition for $GaAs_xSb_{1-x}$

show single phase solid solubility over the complete range of x; it has a miscibility gap in the range $0.38 < x < 0.61$ (73G). Thus the investigation of band gaps and their semiconductor properties is limited to the composition range in which single phase behaviour exists. The alloys of the system $GaAs_xSb_{1-x}$ have a direct band gap and alloys of this type are becoming increasingly important in new technological developments because of their possible application in optical communication systems (77N - 75N1) where their energy gap values are of particular interest. The room temperature band gap of $GaAs_xSb_{1-x}$ was reported by Thomas and Woolley (70T) and their results are shown in Figure (I-5). The value of E_o at room temperature changes from 0.73 eV to 0.71 eV in the composition range $0 < x < 0.38$ and 0.86 to 1.43 eV from $0.61 < x < 1.0$.

Considerable progress has been made recently in the investigation of the properties of $GaAs_xSb_{1-x}$ from measurements of electrical and high pressure effect (75R), phase diagram (73G), Faraday effect (76D), photoconductivity (70A), light emitting diodes (75N1, 75N2) and finally, in this project plasma reflection measurements to obtain the values of dielectric constant and effective mass value as a function of composition. More recently some work has been reported (72N2) on the quaternary alloys $Al_xGa_{1-x}As_ySb_{1-x}$ at small values of x. The variation of energy gap was examined and it was found that the replacement of small amounts of Ga by Al in $GaAs_xSb_{1-x}$ increased the band gap but that the lattice parameter was practically unchanged. This latter result is of interest technologically in growth problems since it allows matching for epitaxial layers of different composition.

CHAPTER II THEORY

Before presenting the experimental work which has been done in this research project, we shall start with a detailed discussion of the band structure of the relevant semiconductor compounds and alloys. As a brief introduction, some critical points of the theory which are related to this project will be reviewed and for other aspects of the topic, references to the literature are given.

II-1 k.p METHOD AND ENERGY BAND THEORY

The Schrodinger equation for the periodic part of the Bloch function U_{nk} can be written in the form

$$HU_{nk}(r) = E_n(k)\, U_{nk} \tag{II-1}$$

For any given k, the set of function U_{nk} is obtained by letting n run over all bands. Let us assume the band edge is non-degenerate and occurs at the centre of the Brillouin zone. Using simple perturbation theory, the energy band from equation (II-1) becomes (66KA)

$$E_n(k) = E_n(0) + \frac{\hbar^2 k^2}{2m} + \frac{\hbar k.P_{nn'}}{m} + \frac{\hbar^2}{m^2} \sum' \frac{k.P_{nn'}(0)\, k.P_{nn'}(0)}{E'_n(0) - E_n(0)} \tag{II-2}$$

where

$$P_{nn'}(k) = \int d^3k\; U_{nk}(r)\, \frac{\hbar}{i}\, U_{n'k}(r) \tag{II-3}$$

Here, we consider interaction between only the conduction and valence bands and neglect the interactions of all other bands. Using the first approximation in equation (II-2), we obtain quantitative values for the energy bands. For simplicity in the calculation, let us denote the two bands by c and v. Setting $P_{cv} = P_{vc} = P$ and taking the zero energy at the bottom of the conduction band $E_c(0) = 0$ and $E_v(0) = -E_o$ (E_o is an energy gap), under this assumption the following condition for eigen energies is obtained (69Z),

$$\begin{pmatrix} -E_o - E + \frac{\hbar^2 k^2}{2m} & (\frac{\hbar}{m})kP \\ (\frac{\hbar}{m})kP & -\varepsilon + \frac{\hbar^2 k^2}{2m} \end{pmatrix} = 0 \qquad \text{(II-4)}$$

If the free electron contribution in equation (II-4) is neglected, the energy band will be obtained in the form

$$E_{c,v} = -\frac{E_o}{2} \pm \left\{ (\frac{E_o}{2})^2 + E_o \frac{\hbar^2 k^2}{2m} \right\}^{\frac{1}{2}} \qquad \text{(II-5)}$$

If the general definition of cyclotron effective mass in equation (I-7) is used,

$$(\frac{m}{m_o^*})_{c,v} = \pm \frac{2P^2}{mE_o} \qquad \text{(II-6)}$$

is obtained. This shows that the effective masses are equal in magnitude for conduction and valence bands but are opposite in sign. Equation (II-6) gives a value of $m_o^* = 0.013\ m$ for InSb, and all assumptions in general will be valid if $E_g << \frac{2P^2}{m}$. The effective mass at the bottom of the conduction band is determined by equation (II-2), where in this case the

linear term in k vanishes because of the symmetry at the band edge and the energy close to the band edge reduces to

$$E_n(k) = E_n(0) + \frac{\hbar^2 k^2}{2m} + \frac{\hbar^2 k^2}{2m} + \frac{\hbar^2}{m^2} \Sigma \frac{k \cdot P_{nn'}(0)\; k \cdot P_{nn'}(0)}{E(0) - E_{n'}(0)} \qquad \text{(II-7)}$$

Equation (II-7) at the band edge is of the form

$$E_n(k) = E_n(0) + \frac{\hbar^2 k^2}{2m_n^*} \qquad \text{(II-8)}$$

where m_n^* is the effective mass.

In general, the effective mass is dependent on direction and we define an inverse effective mass tensor $(1/m_n)_{\alpha\beta}$; $\alpha, \beta = x, y, z$ for the band n by

$$\left(\frac{1}{m}\right)_{\alpha\beta} = \frac{1}{m} \delta_{\alpha\beta} + \frac{2}{m^2} \sum_{n' \neq n} \frac{P_{nn'}(0)\; P_{n'n}(0)}{E_n(0) - E_{n'}(0)} \qquad \text{(II-9)}$$

so that the energy band becomes

$$E_n(k) = E_n(0) + \frac{\hbar^2}{2} \Sigma\, k_\alpha \left(\frac{1}{m_n}\right)_{\alpha\beta} k_\beta$$

close to the band edge and the shape of the band is completely described by the components of the inverse effective mass tensor defined in equation (II-9). For a degenerate band edge, we cannot write down explicit expressions for the energy as a function of k and usually this is represented in terms of matrix elements. Kane (57K) used first order perturbations in his calculation and obtained the eigen function of the operator H in the form

$$H = \frac{p^2}{2m} + V(r) + \frac{\hbar^2}{4m^2c^2} \sigma \cdot (\nabla V \times P) \qquad \text{(II-10)}$$

where V(r) is a periodic potential, P is the momentum operator, σ is the Pauli spin operator, and m is the free-electron mass. The eigenfunctions of the Hamiltonian (II-10) are Bloch functions of the form

$$\psi_k(r) = U_k(r) \exp(ikr)$$

Kane used this basic idea and developed a theoretical calculation of the band form by including the symmetry properties of the wave function in his analysis to obtain quantitative values for the band structure parameters.

II-2 KANE THEORY

According to the Kane theory (57K), the interaction between the conduction band around the (000) minimum and the three valence bands determines the separation and shape of the conduction and valence bands. The parameters in the Kane semi-quantitative theory are: the separation between the valence bands and conduction band E_o, the matrix element of linear momentum P for coupling between the conduction band and valence bands and the spin orbit splitting of the valence bands Δ_o, i.e.

$$P = -i \frac{\hbar}{m} \langle s | P_z | z \rangle \qquad \text{(II-11)}$$

$$\Delta_o = \frac{3\hbar c}{4m_o^2 c^2} \langle x | (\nabla V \times P)_z | Y \rangle \qquad \text{(II-12)}$$

where s refers to the two $s_\pm$ functions representing the conduction band, and x, y, z refer to $x_\pm$, $y_\pm$ and $z_\pm$, i.e. the six P functions representing

the valence bands, the ± corresponding to spin up and spin down. Under these assumptions, Kane found an 8 x 8 matrix for interaction of the conduction and valence bands and obtained a cubic equation which determines the energy of the electrons as a function of the wave vector k. i.e.

$$E(E + E_o)(E + E_o + \Delta_o) - P^2k^2(E + E_o + 2\Delta_o/3) = 0 \qquad \text{(II-13)}$$

where

$$E = E(0) - \frac{\hbar^2k^2}{2m} = E(0) - ak^2$$

Different approximations have been used to solve the Kane equation (64M). In order to find a general solution for the conduction band, we use the definition of cyclotron effective mass (equation I-7).

Let the zero of energy be at the bottom of the conduction band (i.e. $E = 0$ when $k = 0$) and $a = \frac{\hbar^2}{2m}$. Under these conditions, the cyclotron effective mass reduces to the bottom of the band mass (m^*_{oo}) and this gives

$$\left(\frac{1}{m^*_{oo}} - \frac{2a}{\hbar^2}\right) E_o(E_o + \Delta_o) = \frac{2aP^2}{3\hbar^2}(3E_o + 2\Delta_o) \qquad \text{(II-14)}$$

or

$$\frac{m}{m^*_{oo}} = 1 + \frac{P^2}{3}\left\{\frac{2}{E_o} + \frac{1}{E_o + \Delta_o}\right\} \qquad \text{(II-15)}$$

$$P^2 = \frac{E_o(E_o + \Delta_o)}{(E_o + 2\Delta_o/3)}\left(\frac{m}{m^*_{oo}} - 1\right) \qquad \text{(II-16)}$$

Substituting equation (II-15) into equation (II-13) the result becomes

$$E(E + E_o) = ak^2E_o\left(\frac{m}{m^*_{oo}} - 1\right)\left(1 + \frac{E}{E_o + 2\Delta_o/3}\right)\left(1 + \frac{E}{E_o + \Delta_o}\right)^{-1} \qquad \text{(II-17)}$$

and under the condition $E << E_o^* + 2\Delta_o/3$, equation (II-17) reduces to

$$E^2 + EE_o - ak^2E_o\left(\frac{m}{m^*_{oo}} - 1\right) = 0 \qquad \text{(II-18)}$$

which is independent of Δ_o. Equation (II-18) can be written in the form

$$E = ak^2 + \frac{E_o}{2}\left[\left\{1 + \frac{4ak^2}{E_o}\left(\frac{m}{m^*_{oo}} - 1\right)^{\frac{1}{2}} - 1\right\}^{\frac{1}{2}} - 1\right] \qquad \text{(II-19)}$$

and using the general definition of cyclotron effective mass,

$$\left.\frac{dE}{dk}\right|_{E=E_f} = 2ak\left[1 + \left\{1 + \frac{4a}{E_o}\left(\frac{m}{m^*_{oo}} - 1\right)k_F^2\right\}^{-\frac{1}{2}}\left(\frac{m}{m^*_{oo}} - 1\right)\right] \qquad \text{(II-20)}$$

is obtained. Substituting k_F from equation (II-85) in equation (II-20), a value for the conduction band effective mass for a highly degenerate semiconductor specimen is obtained (69T) in the form

$$\left(\frac{m}{m^*_o}\right) = 1 + \left(\frac{m}{m^*_{oo}} - 1\right)\left\{1 + \frac{4a}{E_o}\left(\frac{m}{m^*_{oo}} - 1\right)(3\pi^2N)^{2/3}\right\}^{-\frac{1}{2}}$$

The Kane analysis applies at zero temperature only. However, Ehrenreich suggested that the Kane theory would still be applicable at higher temperatures if E_o is replaced by E_o^*, the effective mass band gap (57E). If the values of E_o^*, the carrier concentration N and the effective mass at the Fermi level (m/m^*_o) are known, the effective mass at the bottom of the conduction band (m/m^*_{oo}) can thus be determined .

II-3 DISORDER EFFECT IN SEMICONDUCTOR ALLOYS

The fundamental problem which arises in the study of alloy systems is that the crystal potential is not periodic. As a result, the condition for the validity of Bloch's theorem are not satisfied and it is no longer possible to characterize the electron state by a wave vector k. Consequently, the energy band and the Brillouin zone lose some of their meaning. However, these alloys show substitutional solid solution with the atoms of the component elements distributed at random over a sublattice of a regular crystal lattice. Thus a considerable degree of order remains and the aperiodic part of the potential is relatively small. All available data on semiconductor alloys indicate that the alloys show very similar physical properties to the compounds and some of their properties vary continuously with composition. For example, Figures (I-5) and (IV-3) show the variation of the energy gap and lattice constant as a function of the mole fraction x of the $GaAs_xSb_{1-x}$ alloys. It is clear therefore that we are justified in attributing definite band structure properties to the alloys despite the presence of some aperiodicity in the potential terms. In general, if the band structures of the semiconductor compounds are known, a qualitative estimate of the band structure of the alloys can be made, but for quantitative data measurements must be made on the alloys

For theoretical analysis of the band structure of semiconductor alloys, the virtual crystal approximation (VCA) method (55P, 70S, 72R2) is widely used. In this model, the random fluctuations of the potential of the component atoms are replaced by a sum of suitable average potentials

having the probabilities x and (1-x). In a later development, the coherent potential approximation (CPA) (70S1, 75K) is a method that makes it possible to treat the single particle properties of disordered alloys within the framework of multiple scattering theory as a succession of scattering processes caused by randomly distributed atomic potentials of the component atoms of the alloy. In this section we shall concentrate on the VCA method, in order to calculate the effective mass value at the bottom of the conduction band using the equation developed by Berolo, Woolley and Van Vechten. They indicated that the effects of disorder in alloys are due to the breaking of the crystal symmetry by the aperiodic terms. Consequently mixing of valence and conduction band states occur, particularly at the Γ point, and they found a quantitative value for the conduction band effective mass as a function of composition, which involved the values of the various valence band masses and the spin-orbit splitting Δ_o.

The experimental values of the conduction band effective mass for the systems $InAs_xSb_{1-x}$ and $Ga_xIn_{1-x}Sb$, $Ga_xIn_{1-x}As$ and also for the systems $GaAs_xSb_{1-x}$ and $Ga_{1-x}Al_xAs$, which are considered in this work, are in agreement with the theoretical calculation of the disorder equation. The effects of disorder in semiconductor alloys on a number of different properties have been investigated recently, e.g. band structure (70S, 75K), effective mass values (73W, 74RO), disorder properties of the energy gap as a function of temperature (74H, 75H), k.p theory in semiconductor alloys (74S), the density of states with a complete list of work on the alloy properties (73Y and 74E), quantitative calculation of the bowing parameter (73S) and various other approaches to disorder properties (77C,

77T). The effect of disorder on the dielectric constant of the alloys $GaAs_xSb_{1-x}$ will be discussed in some detail in the following section.

II-4 VIRTUAL CRYSTAL APPROXIMATION (VCA)

Let us consider the binary solid solution A_xB_{1-x} whose atoms are randomly distributed on lattice sites of a simple Bravais lattice. The potential energy term in the one-electron Hamiltonian is

$$H = -\frac{\hbar^2}{2m}\nabla^2 + V(r) \qquad \text{(II-21)}$$

In the VCA, V(r) is the actual potential and can be replaced on each lattice site by the weighted average potential V^{vc} defined (55P) by

$$V^{vc}(r - R_\ell) = x\,V^A(r - R_\ell) + (1 - x)V^B(r - R_\ell) \qquad \text{(II-22)}$$

where $V^A(r - R_\ell)$ and $V^B(r - R_\ell)$ are potential terms corresponding to atoms of the type A and B centred at R with probabilities x and 1 - x. The corresponding Hamiltonian is

$$H^{vc} = -\frac{\hbar^2}{2m}\nabla^2 + \sum_\ell V^{vc}(r - R_\ell) \qquad \text{(II-23)}$$

Equation (II-21) can now be rewritten in the following form:

$$H = H^{VC} + V(r) - V^{VC}(r - R_\ell) = H^{vc} + U$$

In this equation, the effect of the aperiodic term due to the disorder of

the lattice has been included. It follows that the VCA may be considered to be the starting approximation for treating alloys disorder. It can be seen from equation (II-23), that the virtual crystal Hamiltonian H^{VC} is periodic with the period of the crystal lattice. The solutions of the Schrodinger equation ψ_{nk}, which are known to be Bloch functions, and the energy eigenvalues $E_n(k)$ can be calculated in the same way as for perfect crystals. However, in the calculation of the energy band structure in semiconductor alloys, the question arises whether and to what extent the usual concepts of band theory based on the translation periodicity of the crystal lattice are preserved. This is one of the complicated problems in semiconductor alloys and certain progress in this problem has been made very recently by Kumar et al. (75K).

II-5 DISORDER EQUATION FOR THE CONDUCTION BAND EFFECTIVE MASS

The analysis on the VCA principle (70B) explains that the energy E_o in semiconductor alloys will not vary linearly with mole fraction x because E_o is not a linear function of the potential for any of the commonly used methods of the band structure calculation. As indicated above, the experimental results (67T, 63C, 57L) confirm this prediction. The form of the variation of the energy gaps in semiconductor alloys was found by Thompson and Woolley (67T). They showed that for most of the direct energy gap of semiconductor alloys the value of E_o has approximately quadratic dependence on the mole fraction x. i.e.

$$E_o(x) = a + bx + cx^2 \qquad \text{(II-24)}$$

where a and b are determined from the band gaps of the parent compounds, but c, the bowing parameter, is characteristic of the alloys. The bowing parameter c_i predicted by Van Vechten and Bergstresser (70B) in their VCA analysis is always positive and the values are found to be different from c. Thus it was suggested that the bowing parameter c was the sum of an intrinsic (virtual-crystal) bowing parameter c_i, determined from the virtual-crystal approximation (70V), and an extrinsic (disorder) parameter c_e due to the effects of the short range aperiodic part of the crystal potential. The value c_e is estimated as $c_e = C_{FG}^2/A$ where C_{FG} is the Phillips electronegativity difference (70P) between the mixed elements F and G and A is a constant bandwidth parameter. Berolo, Van Vechten and Woolley (71W) examined the variation of the spin orbit splitting $\Delta_o(x)$ of the valence band at the Γ point, and of $\Delta_1(x)$, the splitting of the L point, as a function of composition x for some III-V alloys. From the VCA model, $\Delta_o(x)$ and $\Delta_1(x)$ should deviate from linearity only to the extend that the overlap of the relevant wave function with the nuclei vary (67B), which is very little, thus the magnitude of the bowing of $\Delta_o(x)$ and $\Delta_1(x)$ must be explained by the aperiodic effect. They also observed, for intermediate compositions, deviations in the values of the conduction band effective mass m^*_{oo} from the predictions of a simple Kane model. This also would be attributed to the same kind of mixing of valence and conduction bands due to the breaking of the crystal symmetry by the aperiodic terms (72W). Thus mixing of the conduction and valence band states occurs at the Γ point, and the resulting conduction band effective mass will be determined to some extent by the valence band effective mass. Woolley, Berolo and Van Vechten (73W) found for the conduction band effective mass value the

following expression

$$\frac{1}{m^*_{oo}} = \frac{1}{m_{co}} + \frac{x(1-x)\ C^2_{FG}}{3A}\left[\frac{1}{m_{hh}E_{ov}} + \frac{1}{m_{lh}E_{ov}} + \right.$$

$$\left. + \frac{1}{m_{so}(E_{ov} + \Delta_{ov})} - \frac{1}{m_{co}}\left(\frac{2}{E_{ov}} + \frac{1}{E_{ov} + \Delta_{ov}}\right)\right] \qquad \text{(II-25)}$$

where E_{ov} and Δ_{ov} are the VCA values and are obtained from Van Vechten and Bergstresser analyses, i.e. E_{ov} is calculated from the values of c_i given by Van Vechten and Bergstresser and Δ_{ov} is assumed linear with x. Similarly m_{hh} and m_{so} are assumed to vary linearly between the values for the compounds. The light hole mass m_{lh} has been assumed to have the same values as m_{co}, which is good approximation in the Kane model (57K). Finally, m_{co} is the effective mass for the conduction band in the absence of conduction-valence band mixing but with all other effects, in particular the true $E_o(x)$, included. Equation (II-25) can be used to predict variation of the conduction band effective mass as a function of mole fraction x and comparison with experimental data gives a good check on the effect of disorder in semiconductor alloys.

II-6 CLASSICAL THEORY OF OPTICAL CONSTANTS

II-61 Maxwell's Equations

The physical properties of the interaction of radiation with a

medium characterized by the permeability constant μ_o, the dielectric constant ε_o of free space and conductivity σ follow from Maxwell's equations

$$\nabla \cdot (\varepsilon_o E + P) = 0 \qquad \text{(II-26)}$$

$$\nabla \cdot H = 0 \qquad \text{(II-27)}$$

$$\nabla \times E = -\frac{\partial}{\partial t} \mu_o H \qquad \text{(II-28)}$$

$$\nabla \times H = J + \frac{\partial}{\partial t} (\varepsilon_o E + P) \qquad \text{(II-29)}$$

where J the current density in terms of electric field is $J = \sigma E$. For cubic crystals, the polarization P is proportional to the field and can be expressed by:

$$P = \varepsilon_c \chi E$$

where χ, a scalar quantity, is called the electric susceptibility. The electric displacement thus becomes:

$$\varepsilon_o E + P = \varepsilon_o (1 + \chi) E = \varepsilon_o \varepsilon E \qquad \text{(II-26a)}$$

which defines the specific dielectric constant ε of the medium. From equation (II-28) and (II-26a), it can be shown that

$$\nabla (\nabla . E) - \nabla^2 E = \mu_o \frac{\partial J}{\partial t} - \mu_o \varepsilon \varepsilon_o \frac{\partial^2 E}{\partial t} \qquad \text{(II-30)}$$

The combination of equations (II-26) and (II-30) gives a transverse plane wave function which represents propagation of radiation in an energy absorbing medium

$$\nabla^2 E = \mu_o \frac{\partial J}{\partial t} - \mu_o \varepsilon \varepsilon_o \frac{\partial^2 E}{\partial t} \qquad \text{(II-31)}$$

In order to solve equation (II-31), consider a single plane wave function within the medium of the form

$$\mathcal{E} = \mathcal{E}_o \exp i(q.r - \omega t) \qquad \text{(II-32)}$$

where $\mathcal{E}_o$ is perpendicular to the wave vector q and ω is the frequency. Substituting equation (II-32) into (II-31) and (II-33),

$$q = \mu_o \frac{\omega^2}{c^2} \left(\varepsilon - \frac{i\sigma}{\omega \varepsilon_o}\right) \qquad \text{(II-33)}$$

is obtained. Now define a complex refractive index $\eta^* = \eta + i\kappa$ (where η is the real part of the refractive index and κ is the extinction coefficient) and obtain expression for ε and σ in terms of η and κ from equation (II-32) and (II-33) of the form

$$\varepsilon_1 = \eta^2 - \kappa^2 \qquad \text{(II-34)}$$

$$\varepsilon_2 = \frac{\sigma}{\omega \varepsilon_o} = 2\eta\kappa \qquad \text{(II-35)}$$

ε is defined by

$$\varepsilon = \varepsilon_1 + i\varepsilon_2 \qquad \text{(II-36)}$$

where ε_1 and ε_2 are real and imaginary parts of dielectric constant and ε is a complex dielectric constant which appears in the usual versions of Maxwell's equations.

II-7 REFLECTIVITY

The reflection coefficient of a perfectly smooth surface material which represents the reflected part of the energy of a normally incident beam, can be expressed in terms of the optical parameters η and κ in the form

$$R = \frac{(\eta - 1)^2 + \kappa^2}{(\eta + 1)^2 + \kappa^2} \qquad \text{(II-37)}$$

and the transmission coefficient of light through a plate of thickness d is given by:

$$T = \frac{(1 - R)^2}{1 + R^2 \exp(-2\alpha d)} \, e^{-\alpha d} \qquad \text{(II-38)}$$

where α is the absorption coefficient, which can be expressed in terms of the extinction coefficient κ, as

$$\alpha = \frac{2\omega}{c} \kappa \qquad \text{(II-39)}$$

The optical parameters η and κ are related to the electrical parameters σ and χ by the relation

$$\varepsilon_1 = \eta^2 - \kappa^2 = 1 + 4\pi\chi$$

$$\varepsilon_2 = 2\eta\kappa = \frac{4\pi\sigma}{\omega} \qquad \text{(II-40)}$$

In the range of wavelength in which the absorption is weak (i.e. α is small), $\kappa \ll (\eta - 1)^2$ and the reflection coefficient (II-37) reduces to

$$R = \left(\frac{\eta - 1}{\eta + 1}\right) \quad \text{or} \quad \eta^2 = \left(\frac{1 - \sqrt{R}}{1 + \sqrt{R}}\right) \qquad \text{(II-41)}$$

Equation (II-41) has been used in this work to analyse data in the range 9 to 30 microns in order to calculate values of dielectric constant and effective mass and other parameters which are related to the band structure of the alloys of the systems $GaAs_xSb_{1-x}$ and $Ga_{1-x}Al_xAs$.

II-8 CLASSICAL PLASMA FREQUENCY

In a one-dimensional model of a solid, let us assume that the electric field has a z-component only and that $\nabla xE = 0$ when $H = 0$. Maxwell's equation (II-29) then becomes

$$J + \varepsilon_o \varepsilon \left(\frac{\partial E}{\partial t}\right) = 0 \qquad \text{(II-42)}$$

and for longitudinal motion we have

$$m\left(\frac{\partial V}{\partial t}\right) = eE \qquad \text{(II-43)}$$

The current density and velocity are related by (59S)

$$J = N\,ev \qquad \text{(II-44)}$$

where N is the equilibrium density of electrons. The relationship between local electron density and electric field given by Poisson's equation is

$$\frac{\partial E}{\partial z} = \frac{1}{\varepsilon} Ne$$

Substituting equations (II-43) and (II-44) into (II-42), we obtain

$$N\,ev + \frac{\varepsilon_o \varepsilon m}{e} \frac{\partial^2 V}{\partial t^2} = 0 \qquad \text{(II-45)}$$

Using equation (II-32) and by replacing $\frac{\partial}{\partial t}$ by $-i\omega$, equation (II-45) reduces to

$$v \{Ne + \frac{\varepsilon_o \varepsilon m}{e} (-\omega)^2\} = 0 \qquad \text{(II-46)}$$

Since v must be finite, and the term in the brackets is independent of wavevector, there is only a single value of ω allowed by equation (II-46) for longitudinal motion. This is called the plasma frequency ω_p and is defined by rearranging equation (II-46) in the form

$$\omega_p^2 = \frac{Ne^2}{m^* \varepsilon_o \varepsilon_\infty} \qquad \text{(II-47)}$$

For a degenerate specimen the dielectric constant may be written in terms of the plasma frequency as

$$\varepsilon_1 = \varepsilon_\infty \left(1 - \frac{\omega_p^2}{\omega^2}\right)$$

$$\varepsilon_2 = \varepsilon_\infty \frac{\omega_p^2}{\omega^3 \tau} \qquad \text{(II-48)}$$

From these equations, it may be seen that for $\omega >> \omega_p$ the imaginary part of the dielectric constant becomes very small and the real part is dominant. For $\omega << \omega_p$, the real part of the dielectric constant is negative and the imaginary part of the dielectric constant will be greater than the real part. It is also seen that as ω approaches ω_p, the real part of the dielectric constant decreases and reaches a minimum when $\omega = \omega_p$. This minimum is referred to as the plasma minimum, and after this minimum the reflectivity usually rises very rapidly. Equation (II-48) may be written for the real part of the dielectric constant ε in

the form

$$\varepsilon = \varepsilon_\infty - \frac{Ne^2}{\varepsilon_o m_s^*} \lambda^2 \qquad \text{(II-49)}$$

where N is the carrier concentration and m_s^* is the susceptibility effective mass. According to equation (II-49), a plot of ε vs. λ^2 should be a straight line and the effective mass value can be obtained from the slope. The second term in equation (II-49) is the free carrier contribution to the dielectric constant and may be denoted by ε_{FC} where

$$\varepsilon_{FC} = - \frac{4\pi c^2 Ne^2}{\omega^2 \varepsilon_o m_s^*} \qquad \text{(II-50)}$$

II-9 DETERMINATION OF SOME OPTICAL PARAMETERS (τ_{opt}, μ_{opt}, σ_{opt} and k_{min})

The basic equations describing the free carrier dispersion in a region where the free carriers of the material interact with the electromagnetic radiation are given as follows (69T, 71D)

$$\varepsilon = \varepsilon_1 + i\varepsilon_2$$

$$\varepsilon_1 = \eta^2 - \kappa^2 = \varepsilon_\infty - \frac{Ne^2}{m_c^* \varepsilon_o} \left\langle \frac{\tau^2}{1 + \omega^2\tau^2} \right\rangle$$

$$\varepsilon_2 = 2\eta\kappa = \frac{Ne^2}{m_c^* \varepsilon_o \omega} \left\langle \frac{\tau}{1 + \omega^2\tau^2} \right\rangle \qquad \text{(II-51)}$$

where ε_1 and ε_2 are the real and imaginary parts of the dielectric constant, m^* is the free carrier conductivity effective mass, N is the free carrier

density and τ is the relaxation time. Phillips (67P) and subsequently Rheinlander (70R) showed that if the intraband free carrier contribution to the dielectric constant is neglected, the left side of the equation (II-51) can usually be replaced by

$$\left\langle \frac{\langle\tau^2\rangle}{1 + \omega^2\tau^2} \right\rangle \simeq \frac{\langle\tau^2\rangle}{1 + \omega^2\langle\tau\rangle^2} = \frac{r^2\langle\tau\rangle^2}{1 + \omega^2 r^2\langle\tau\rangle^2} \qquad \text{(II-52)}$$

where $r^2 = \langle r^2\rangle / \langle r\rangle^2$ is the Hall scattering coefficient for the material and $\langle\tau\rangle$ is the averaged carrier relaxation time. From (II-52), equations (II-47) and (II-51) can be written in the form

$$\frac{\varepsilon_\infty + \kappa^2 - \eta^2}{\varepsilon_\infty} = \frac{\omega_p^2}{\omega^2 + r^{-2}\langle\tau\rangle^{-2}} \qquad \text{(II-53)}$$

$$2\eta\kappa r^2\omega\langle\tau\rangle = \frac{\omega_p^2}{\omega^2 + r^{-2}\langle\tau\rangle^{-2}}$$

$$\omega\langle\tau\rangle = \frac{(\varepsilon_\infty + \kappa^2 - \eta^2)}{2\eta\kappa\, r^2} \qquad \text{(II-54)}$$

Substituting equation (II-54) into equation (II-53), the result becomes

$$\omega_p^2 = \left(\frac{\varepsilon_\infty + \kappa^2 - \eta^2}{\varepsilon_\infty}\right)\omega^2 + \frac{\varepsilon_\infty + \kappa^2 - \eta^2}{r^2\langle\tau\rangle^2\,\varepsilon_\infty}$$

or

$$\frac{\omega_p^2}{\omega^2} = \left(\frac{\varepsilon_\infty + \kappa^2 - \eta^2}{\varepsilon_\infty}\right) + \frac{4\eta^2\kappa^2 r^2}{\varepsilon_\infty\,(\varepsilon_\infty + \kappa^2 - 2)} \qquad \text{(II-55)}$$

To find an interrelation between η and κ at the minimum reflectivity, manipulation of equations (II-54) and (II-55) to eliminate ω leads to

$$(\varepsilon_\infty - \eta^2 + \kappa^2)\left\{ r^2 + \frac{(\varepsilon_\infty - \eta^2 + \kappa^2)^2}{4\eta^2\kappa} \right\} = \frac{r^4 Ne^2 \langle\tau\rangle}{m_s \varepsilon_o}$$

$$= \text{constant} \qquad \text{(II-56)}$$

and the reflectivity is defined by

$$R = \frac{(\eta - 1)^2 + \kappa^2}{(\eta - 1)^2 + \kappa^2} \quad \text{or} \quad \frac{1 + R}{1 - R} = \frac{\eta^2 + \kappa^2 + 1}{2\eta} \qquad \text{(II-57)}$$

By differentiating $(1 + R)/(1 - R)$ with respect to κ^2 on both sides of equation (II-57) we obtain

$$\frac{d\eta}{d\kappa^2} = \frac{\eta}{1 + \kappa^2 - \eta^2} \qquad \text{(II-58)}$$

and by differentiating equation (II-56)with respect to κ^2 we have

$$\frac{d\eta}{d\kappa^2} = \frac{\eta}{2\kappa^2}\left\{ \frac{2\kappa^2 + 3\varepsilon_\infty + (4r^2 - 3)\kappa^2 - (\varepsilon_\infty - \eta^2)^3}{\{2\eta^2 - 3\varepsilon_\infty + (4r^2 - 3)\}\eta^4 + (\varepsilon_\infty + \kappa^2)^3} \right\} \qquad \text{(II-59)}$$

From equations (II-58) and (II-59), the following interrelation between η and κ at the minimum reflectivity can be obtained

$$\kappa^2(5\eta^2 + 3\varepsilon_\infty - 2) = (\varepsilon_\infty - \eta^2)(\eta^2 - 1) - \frac{4\eta^2\kappa^4 r^2(3\eta^2 - \kappa^2 - 1)}{(\varepsilon_\infty - \eta^2 + \kappa^2)^2} \qquad \text{(II-60)}$$

in which the last term on the right hand side of the equation can be neglected if $\omega^2\tau^2 \gg 1$. Therefore, at the minimum reflectivity, equation (II-60) can be written in the form

$$\kappa^2_{min} = \frac{(\varepsilon_\infty - \eta^2_{min})(\eta^2_{min} - 1)}{(5\eta^2_{min} + 3\varepsilon_\infty - 2)} \qquad \text{(II-61)}$$

and $\mu_{opt} = \frac{e\tau}{m^*}$

$$\sigma = ne\,\mu_{opt} = \varepsilon_\infty \varepsilon_o \omega_p^2 \tau$$

Thus τ, μ_{opt}, κ_{min} and σ can be calculated from the values at the minimum of the plasma reflection.

STATISTICAL THEORY

II-10 BOLTZMAN EQUATION

The distribution of electrons in energy in accordance with the Fermi-Dirac function is valid only for a system in thermodynamical equilibrium. When a force is applied to a solid, the distribution function must be modified to take into account small deviations from equilibrium. This is done by use of the Boltzmann equation.

According to the electron theory, for crystals which have spherical symmetric energy surfaces, the electron distribution function f in a stationary state is determined as a new distribution function of the state k of the electron and time using the Boltzmann equation (59S)

$$\frac{e}{h} \cdot \frac{df}{dE} \; (F \cdot \nabla_k E) = \left\{ \frac{df}{dt} \right\}_{coll} = - \frac{f - f_o}{\tau} \qquad \text{(II-62)}$$

In this equation, f_o is the distribution function at the corresponding thermal equilibrium state and τ is a relaxation time. The value $\{\frac{df}{dt}\}_{coll}$ is the difference between the number per unit time of particles whose

wave vectors change to k due to scattering and the number of particles whose wave vectors change from k to some other wave vector due to the scattering mechanism. Assuming that the disturbance is small, so that $\frac{\partial f}{\partial E}$, can be replaced by $\frac{df_o}{dE}$, that $f - f_o = \Delta f$ and $F = -eE$ where E is the electric field, equation (II-62) can be written as

$$\Delta f = \frac{e}{h} \tau E \frac{\partial f_o}{\partial E} \nabla_k E \qquad \text{(II-63)}$$

When the electric field varies with time according to

$$\mathcal{E}_x = \mathcal{E}_o \exp(i\omega t) \qquad \text{(II-64)}$$

then equation (II-63) can be written as (36W1)

$$\Delta f_1 \simeq \frac{1}{i\omega\tau + 1} \Delta f \qquad \text{(II-65)}$$

where Δf_1 is a solution for the alternating electric field given by equation (II -64).

II-11 STATISTICAL THEORY OF FREE CARRIER REFLECTIVITY

The current density in the x direction in terms of the distribution function f is given by (57F, 69T)

$$J = -\frac{2}{(2\pi)^3} e \int \Delta f_1 V_x \, d\Omega_k \qquad \text{(II-66)}$$

where V_x is electron velocity in the x direction and $d\Omega_k = dk_x dk_y dk_z$ is a volume element in k space. Equation (II-66) may be rewritten in terms of

equation (II-65) in the form

$$J_x = -\frac{e^2}{4\pi^3\hbar}\int E_x \frac{\tau V_x}{1 + i\omega\tau}\frac{\partial f_o}{\partial k_x}\, d\Omega_k \qquad \text{(II-67)}$$

By substituting the relations

$$\frac{\partial E}{\partial t} = i\omega E_x \qquad \text{and } V_x = \frac{1}{\hbar}\frac{\partial E}{\partial k_x} \qquad \text{(II-68)}$$

equation (II-67) becomes

$$J_x = -\frac{e^2}{4\pi^3\hbar}\left\{E_x \int \frac{\tau V_x}{1 + \omega^2\tau^2}\frac{\partial f_o}{\partial k_x}\, d\Omega_k - \frac{\partial E_x}{\partial t}\int \frac{\tau^2 V_f}{1 + \omega^2\tau^2}\frac{\partial f_o}{\partial k_x}\, d\Omega_k\right\} \qquad \text{(II-69)}$$

In the alternating electric field, the current density J can be represented formally as the sum of a conduction current, varying in phase with the electric field, and a displacement current, lagging in phase behind the field by $\pi/2$ for a crystal of cubic symmetry, i.e.

$$J = \sigma E + \chi \frac{\partial E}{\partial t} \qquad \text{(II-70)}$$

where σ and χ represent the conductivity and electrical susceptibility. Comparison with equation (II-69) and (II-70) leads to

$$\sigma = -\frac{e^2}{\hbar}\int \frac{\tau v_x}{1 + (\tau\omega)^2}\frac{\partial f_o}{\partial k_x}\frac{2}{(2\pi)^3}\, d\Omega_k \qquad \text{(II-71)}$$

and

$$\chi_c = \frac{e^2}{4\pi^3\hbar} \int \frac{\tau v_x}{1 + (\tau\omega)^2} \frac{\partial f_o}{\partial k_x} \, d\Omega_k \qquad \text{(II-72)}$$

In a static electric field, the conductivity represents the value of the current of free electron charges and the value of the electric susceptibility represent the displacement of bound charges.

In the case $\omega^2\tau^2 >> 1$, equation (II-71) can be rewritten in the form

$$\chi_{FC} = - \frac{e^2}{4\hbar\pi^2\omega^2} \int \frac{\partial V_x}{\partial k_x} f_o \, d\Omega_k \qquad \text{(II-73)}$$

Integrating by parts, we obtain

$$\chi_{FC} = - \frac{e^2}{4\hbar^2\pi^2\omega^2} \left[\int \left\{ V_x f_o \right\}_{k_x = -\infty}^{k_x = +\infty} dk_y dk_z - \int \frac{\partial V_x}{\partial k_x} f_o \, d\Omega_k \right] \qquad \text{(II-74)}$$

and substituting equation (II-68) into (II-74) gives

$$\chi_{FC} = - \frac{e^2}{4\hbar^2\pi^3\omega^2} \int \frac{\partial^2 E}{\partial k_x^2} f_o \, d\Omega_k \qquad \text{(II-75)}$$

For a crystal with cubic symmetry, the susceptibility is independent of direction, hence equation (II-75) may be written

$$\chi_{FC} = \frac{e^2}{4\pi^3\hbar^2\omega^2} \int \frac{1}{3} \nabla_k^2 E \, f_o \, d\Omega_k \qquad \text{(II-76)}$$

The terms inside the integral can be expanded in spherical polar coordinates. Since the angular terms vanish, we have

$$\chi_{FC} = \frac{e^3}{3\pi^2\hbar^2\omega^2} \int_0^\infty \nabla_k (k^2 \nabla_k E) f_o dk \qquad \text{(II-77)}$$

and integrating by parts,

$$\chi_{FC} = \frac{e^2}{3\pi^2\hbar^2\omega^2} \left[\left\{ f_o k^2 \nabla_k E \right\}_{k=0}^{k=\infty} - \int_0^\infty k^2 \nabla_k f_o \nabla_k E dk \right] \qquad \text{(II-78)}$$

In equation (II-78), the first term is zero and after changing the integration variable in the second term, we have

$$\chi_{FC} = - \frac{e^2}{3\pi^2\hbar^2\omega^2} \int_0^\infty k^2 \nabla_k E \nabla_k f_o dE \qquad \text{(II-79)}$$

and the free carrier contribution to the real part of the dielectric constant is expressed by

$$\varepsilon_{FC} = \frac{\chi_{FC}}{\varepsilon_o} \qquad \text{(II-80)}$$

In the spectral range of interest to the present work, the total dielectric constant of the crystal is expressed by

$$\varepsilon = \varepsilon_\infty + \varepsilon_{FC} + \varepsilon_{LV} \qquad \text{(II-81)}$$

where ε_{LV} is called lattice reflection and expressed by

$$\varepsilon_{LV} = \frac{(\varepsilon_\infty - \varepsilon_c)\ \omega_t^2}{\omega_t^2 - \omega^2 - i\gamma\omega} \qquad \text{(II-81a)}$$

where ω_t is the transverse optical phonon frequency and γ is the lattice damping constant. By substituting equation (II-79) and (II-80) into (II-81) we have

$$\varepsilon = \varepsilon_\infty - \frac{e^2}{3\pi^2\hbar^2} I - \varepsilon_\infty \frac{(\varepsilon_c - \varepsilon_\infty)\ \omega_t^2}{\omega_t^2 - \omega^2 - i\gamma\omega} \qquad \text{(II-82)}$$

where

$$I = \int_o^\infty k^2 \nabla_k E \nabla_k f_o \, dE$$

$$f_o = \{1 + \exp\left(\frac{E - E_f}{k_B T}\right)\}^{-1} \qquad \text{(II-83)}$$

and

$$\nabla_E f_o = \frac{1}{k_B T}\{2 + \exp\left(\frac{E - E_f}{k_B T}\right) + \exp\left(\frac{E_f - E}{k_B T}\right)\}^{-1} \qquad \text{(II-84)}$$

Thus as is seen from equation (II-82), the present analysis shows that the real part of the dielectric constant is dependent on the frequency of the incident radiation and also on the energy band of the material.

II-12 CARRIER CONCENTRATION

The total concentration of electrons in the conduction band of a single band material is obtained in terms of a statistical distribution by integrating $f_o \, g(k) d\Omega_k$ between the lower and upper limits of the band, where f_o is the Fermi-Dirac distribution function (equation II-83) and g(k) is the density of states, i.e., the number of states per unit volume of crystal in the range k to k + dk. The total carrier concentration of the conduction band is determined by

$$N = \int_{E_c} g(k) \, f_o \, d\Omega_k \qquad \text{(II-85)}$$

Let us integrate equation (II-85) over the entire band for the case of a spherical energy surface, taking the zero of energy at the bottom of the conduction band and using ∞ as the upper limit of the conduction band,

since the Fermi function goes very rapidly to zero as a function of E, hence it makes no difference how high the upper limit is taken. In equation (II-85) using $g(k) = 2/(2\pi)^3$ as the number of states per unit volume and with the terms inside the integral $d\Omega_k$ expanded in spherical polar co-ordinates, we have

$$N = \frac{1}{\pi^2} \int_o^\infty f_o k^2 dk \qquad \text{(II-86)}$$

By integrating equation (II-86) by parts, changing the variable of integration from dk to dE we obtain

$$N = \frac{1}{3\pi^2} \int_o^\infty k^3 \frac{\partial f_o}{\partial E} dE \qquad \text{(II-87)}$$

For a strongly degenerate specimen, no integration is necessary since $\frac{\partial f_o}{\partial E}$ reduces to a δ function at E_f and the carrier concentration is given by

$$N = \frac{k_f^3}{3\pi^2}$$

where k_f is the wavevector corresponding to the Fermi energy E_f.

CHAPTER III DESIGN AND INSTRUMENTS

III-1 APPROACH TO THE DESIGN

A Baird monochromator was used to measure the room temperature reflectivity of the alloys $GaAs_xSb_{1-x}$ and $Ga_{1-x}Al_xAs$. The monochromator was previously used in a single beam operation with an upper wavelength limit of 16 μm. For the essential part of this project, the operation of the monochromator was changed from single beam to double beam operation to facilitate the measurement of the plasma reflection and also the upper wavelength limit was extended up to 30 μm to allow values of effective mass for the two pseudobinary alloys $GaAs_xSb_{1-x}$ and $Ga_{1-x}Al_xAs$ to be determined.

According to equation (II-49), the square of the plasma resonance frequency is directly proportional to the carrier concentration and inversely proportional to the effective mass. For the alloys to be investigated, in order to bring this resonance frequency close to the available wavelength range, it was necessary to use very large values of carrier concentration N. However the technical difficulties of crystal growth set an upper limit to N. Thus it was necessary to extend the upper wavelength limit of the spectrometer, in order to cover a wavelength range in which the effects of the conduction electrons on the reflectivity could be observed for samples of relatively low carrier concentration. In this way, measurement could be made on samples available in the physics department.

Extension of the upper wavelength limit of the monochromator required readjustment of the setting of the prism and Littrow mirror system. Various settings were tried and for each arrangement the wavelength calibration was checked by observing absorption lines of polystyrene and $PtCl_4$ films. A wavelength of 30 μm was chosen as the upper wavelength limit of the monochromator and with this setting, the lower wavelength limit was found to be 9 μm. This range was quite satisfactory for the proposed measurements since in all cases it allowed data to be obtained from which the graph of ε vs. λ^2, described in equation (II-49), could be drawn and values of m_s^* determined. The advantage of this wavelength extension can be illustrated by considering a $GaAs_xSb_{1-x}$ alloy with $x = 0.04$. With an upper wavelength limit of 16 μm, the minimum carrier concentration which could be used was 7×10^{18} cm^{-3}, which was difficult to obtain. However with the extended wavelength range, the minimum required carrier concentration was reduced to $2 \times 10^{17} cm^{-3}$, which was easily obtained. For sample of higher effective mass, the minimum carrier concentration was correspondingly increased, and the extended wavelength range was of still greater importance.

Some of the electrical and optical instruments used in the double beam arrangement for this experiment were built in the physics department. The following section deals with the research and development of the basic method of the double beam operation which was carried out in this project, and also gives a general account of the final spectrometer arrangement.

III-2 OPTICAL DOUBLE BEAM ARRANGEMENT

A Globar was used as the main source of radiation in the infrared range up to 30 μm. It is a silicon carbide rod of ¼ inch diameter and 4 inches in length that can be electrically heated by a constant voltage transformer to about 1200°C with approximately 300 watts input. The Globar was surrounded by a water cooled jacket with one window, about 1 x 3 cm^2, to safeguard the main source and to keep the temperature constant around the Globar. Radiation passing through the window was collected by the mirror M_1 (see Figure III-1) with a 20 cm focal length and 10 cm diameter and focussed on to the entrance slit of the monochromator. The radiation was then reflected by a plane mirror M_2 inclined at 45° with respect to the incident radiation and sent to a collimator mirror M_3 of 70 cm focal length. This mirror was used firstly to send a parallel beam to the prism and, after the required wavelength of radiation has been selected by the littrow mirror M_4 and prism combination, it focussed the parallel beam returning from the prism on to the exit slit via reflection at a plane mirror M_5. The selection of wavelength was carried out by rotation of the littrow mirror, the angular position of which was controlled by the rotation of a calibrated wavelength drum.

The entrance and exit slits and also the littrow mirror were controlled by the slit cam and the wavelength cam respectively. These two cams were moved synchronously by rotation of the wavelength drum. In the short wavelength range, where the source intensity was high, narrow exit slits were used to increase the resolution of the measurement. In

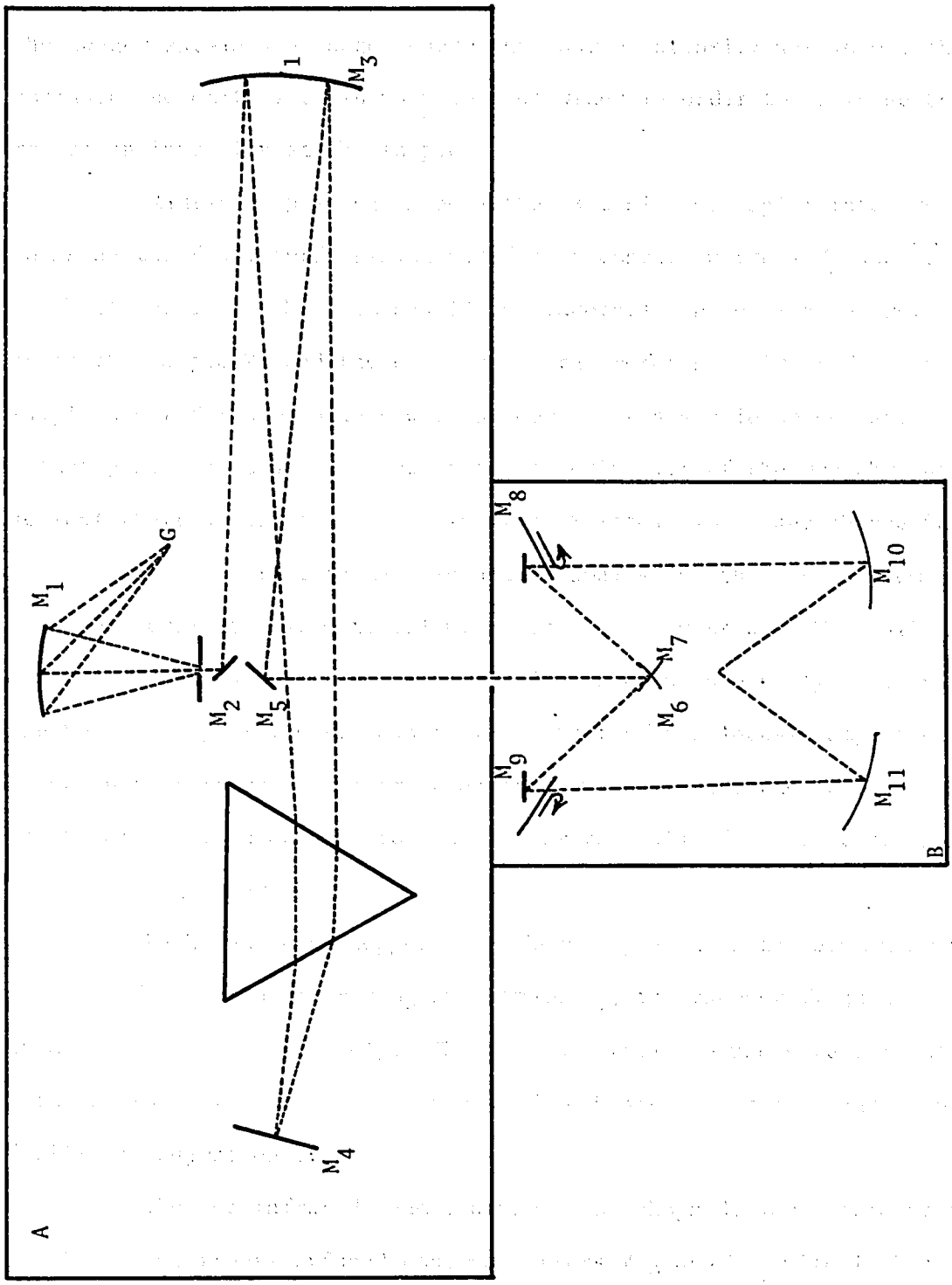

Figure (III-1): Optical monochromator (A) and optical double beam arrangement (B)

the longer wavelength range, where the source intensity was lower, the entrance and exit slit widths were made wider in order to increase the radiation intensity at the sample.

Radiation passing through the exit slit was split into two beams by two front surface-aluminized half-concave mirrors M_6 and M_7 (each of focal length 25 cm and 10 cm diameter), one beam being refocussed on to the sample M_8 and the other on to the reference mirror M_9. The sample and reference holders were supported by a single holder and situated at a suitable distance from the exit slit of the monochromator so that their angle of incident was approximately 10^{o}. Any change in the radiation source affected the two beams equally, so that the system remained completely symmetrical with respect to emission. The ratio of integrated intensity of two beams could have been made unity, but go get the best voltage ratio signals in the output of the lock-in amplifiers, it was better to use a higher integrated intensity for the beam chopped at the higher frequency to compensate for the fall off in detector response with chopping frequency.

Each beam was chopped by a chopper placed in the beam near to the surface of the plane mirror M_9 and sample M_8, the chopper frequencies being 26 Hz and 71 Hz respectively. The two adjustable choppers were mounted on a rubber table to reduce the effects of mechanical vibration and also to facilitate adjustment.

The two infrared beams, after being chopped, were incident on two identical front-surfaced concave mirrors M_{10} and M_{11} with 12.5 cm focal length and 10 cm diameter. The radiation reflected from mirrors M_{11} and M_{12} was refocussed onto a highly sensitive pyroelectric detector

with a KBr window. This window had high transparency up to 40 μm.

The pyroelectric detector (TGS crystal) is a thermal detector with uniform response in the wavelength range 2 to 40 μm with low noise.

All the components of the optical double beam arrangement were mounted on one frame to facilitate adjustment. Each optical component, i.e. mirror, sample, detector, was mounted on a separate holder which was movable on the frame. Each holder was designed to give all required degrees of freedom to the component, i.e. rotation as well as three dimensional linear adjustment. To ensure that the optical system and detector and final focussing mirror system remained fixed, each holder could be locked in position after adjustment. The optical system, the chopper system and the detector were surrounded by a styrofoam box ($1 \times 1 \times 0.5\ m^3$) to screen them from draughts, temperature fluctuations, etc. This decreased the noise picked up by the detector and also isolated the optical system from the environment and consequently increased the voltage signal-to-noise ratio during the measurement.

III-3 OPTICAL PREPARATION

Due to the poor transmission of glass in the infrared range, it was necessary to use mirrors giving reflection from the front face. For this purpose, pure aluminum was chosen as the reflecting material, because it has constant, high reflectivity in the infrared range and also high thermal conductivity.

The procedure for aluminising an optical surface has been

described by Bennett (62B) and was followed here, all mirrors in the double beam system being treated this way. The surface of each glass mirror was cleaned with agua regia (3HCl, 1HNO_3), and then rinsed successively in acetone, deionised water and finally methanol to completely remove all grease, dust, etc. The aluminum layer was produced by vacuum evaporation, the Veco Model, VE-400 evaporator being used for this purpose.

The aluminum to be evaporated, in the form of short rods, was placed in a tungsten basket filament (diameter 1 cm) which could be heated electrically and the glass mirror was held about 30 cm above this filament. The whole system was covered by an inverted glass bell jar which seated on a rubber gasket to give a vacuum-tight contact with the base plate through which the various connections were made. The system was evacuated for about 15 minutes to give a pressure of about 10^{-4}Pa. and then the filament current was slowly raised until the aluminum melted and evaporation onto the mirror occured. After the filament current was turned off, the system was left for 10 minutes before air was admitted into the bell jar. This allowed the mirror and its aluminum film to cool down and avoided any excess oxidation of the aluminum. The mirror was then removed from the system, great care being taken to avoid any contact with the aluminized surface.

III-4 ELECTRICAL ARRANGEMENT

As shown in the block diagram (III-2), the Globar radiation was

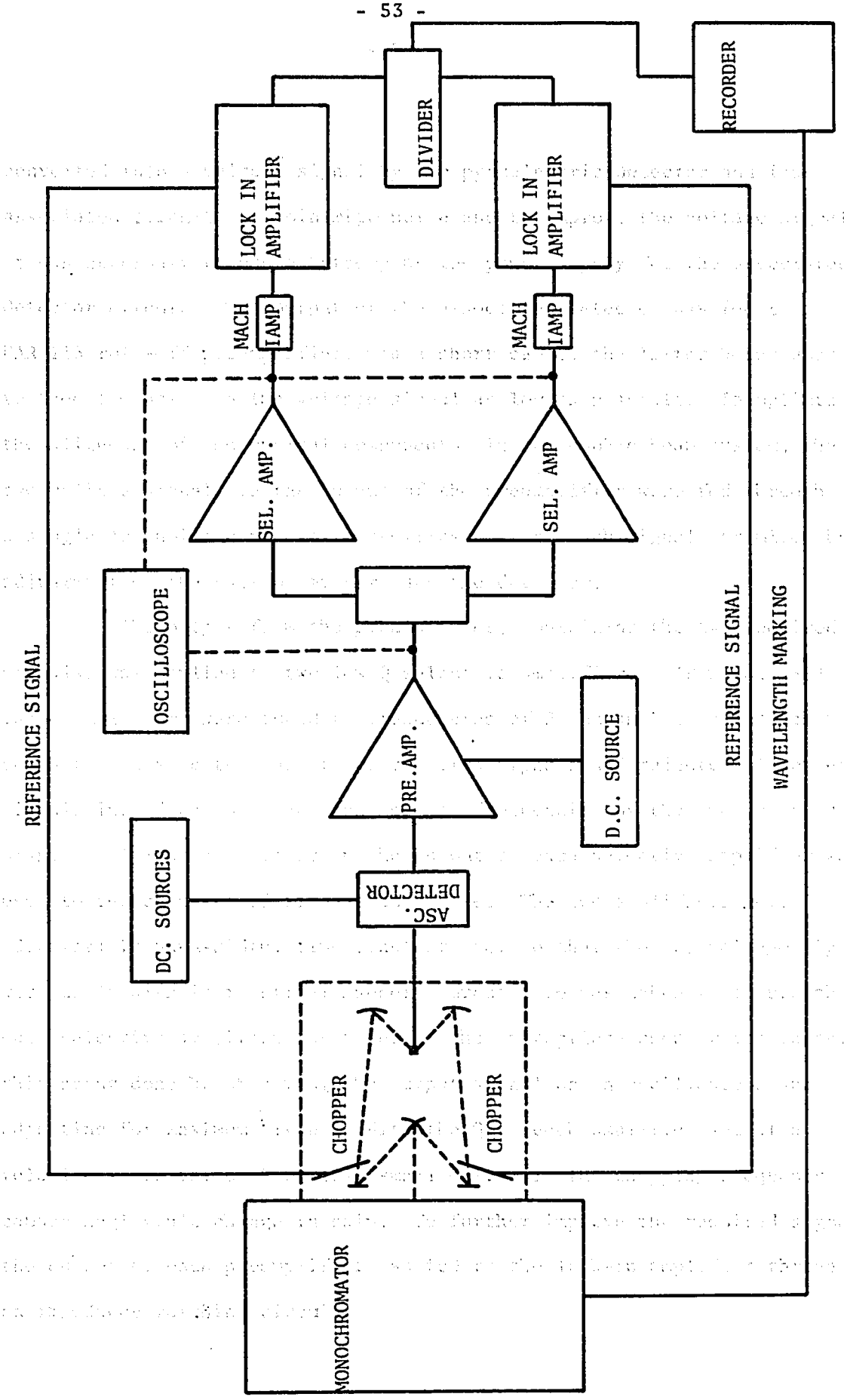

Figure (III-2): Electrical Double Beam Arrangement for Infrared Reflectivity Measurement.

converted into a voltage signal by the pyroelectric detector and its associated circuit. To minimize noise and to improve the voltage signal, it was necessary to use a battery as the power supply for the associated detector circuit. The output of the associated detector was fed to a PAR 113 roll-off preamplifier, via a short cable, the latter being used to keep the noise in the voltage signal as low as possible. To optimize the alignment of the optical components in the double beam system, the two voltage signals in the output of the preamplifier were fed through a single low noise cable to an oscilloscope and each signal maximized by adjustment of the various mirrors and the detector.

The output from the preamplifier, containing the two required signals, was applied to two low Q selective amplifiers (PAR model 189). These amplifiers were tuned to frequencies of 26 Hz and 71 Hz respectively so that each selected one of the required signals and rejected all other signals including noise and combination frequencies of the two unwanted signals. A low-pass filter in the output of each selective amplifier was used to reduce unwanted signals and noise. The two amplifiers were identical in band-width, time constant etc. so that the two voltage signals were dealt with in identical manner. Great care was taken to ensure that each selective amplifier was tuned to the appropriate chopper frequency, this being done by observing the output signal on an oscilloscope and adjusting for maximum signal. With the Q of each amplifier set at a relatively low value (5 or 10), small drifts in the chopping frequency caused negligible change in gain. To further improve the required signal, the output of each preamplifier was fed to the lock-in amplifier through an impedance matching circuit.

The two lock-in amplifiers used were one PAR. model 126 and one PAR. model 186. In the input of each lock-in amplifier, a low pass filter was used to reduce further unwanted signals and noise. A 3 sec. time constant was selected for each lock-in amplifier to obtain identical characteristics and to avoid relative phase shifts between the two systems during the measurements. Each lock-in amplifier requires a reference signal of the appropriate frequency and phase and this was provided from the chopper system, the signal being fed to the lock-in amplifier through a low noise cable. In the output stage of the lock-in amplifiers, the signal is rectified and the output consists of a d.c. voltage proportional to the input signal. The output from the two lock-in amplifiers were fed into a PAR. model 193 voltage divider, the output of which was proportional to the ratio of the two input signals. The time constant control on the divider was set at 3 sec., the same value as for the lock-in amplifiers. The output of the divider was fed into a Honeywell chart recorder.

The chopping frequencies of 26 Hz and 71 Hz were chosen to avoid as much as possible any unwanted pick-up at the general line frequency of 60 Hz or its harmonics. 60 Hz interference was further reduced by using a d.c. power supply for the dtector. Also, a voltage regulator circuit was used for the chopper systems to give stable reference voltage and this also reduced noise in the input signals.

III-5 DESIGN OF CHOPPER AND DRIVER CIRCUIT FOR THE DOUBLE BEAM ARRANGEMENT

The chopper frequency used in the signal beam operation of the Baird spectrometer was chosen to suit the slow response time of a thermocouple detector. Substitution of a pyroelectric detector to obtain higher sensitivity in a spectrum up to 30 μm with double beam operation allowed a higher chopping frequency to be used which gave a better signal to noise ratio. This improvement in performance at high frequencies was due to the faster response in the pyroelectric detector, this giving a smaller current noise during the measurements.

III-51 Control Circuit of Chopper Drive

The chopper system used in this project was designed and set-up in the physics department. Each chopper consisted of a blade with a diameter of about 6 cm mounted on a driver motor which had its spindle connected through a flexible coupling to that of an identical motor used as a generator. Each driver motor was stabilized by a negative feed back circuit (Fig. III-3), the fed-back voltage being the DC voltage from the generator. The generator voltage was compared with a chosen voltage developed across R_2 and the difference gave the input signal to an differential amplifier (DAM). The output of the DAM was applied to the driver current amplifier B (a transistorized Darlington pair), the output of which powered the driver motor M. Any change in the speed of the motor resulted

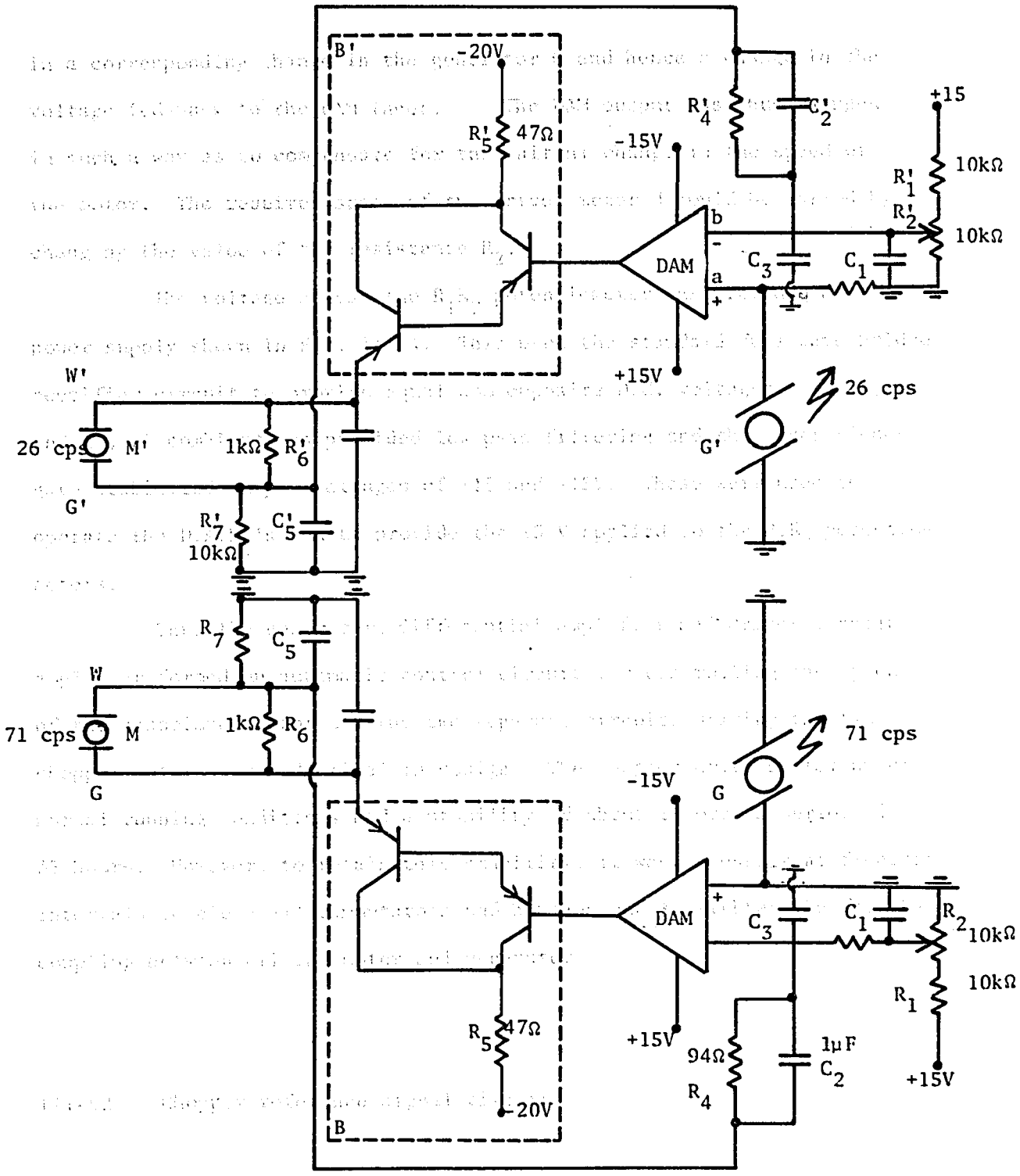

Figure (III-3): Control circuit for the choppers driver with the frequencies 26 cps and 71 cps.

in a corresponding change in the generator G and hence a change in the voltage fed-back to the DAM input. The DAM output was thus changed in such a way as to compensate for the initial change in the speed of the motor. The required speed of the driver motor M could be varied by changing the value of the resistance R_2.

The voltage across the R_1R_2 potentiometer was provided by the power supply shown in Fig. III-4. This used the standard full wave bridge rectifier circuit to provide equal and opposite D.C. voltages. The R, C and R', C' combinations provided low pass filtering and the zener diodes gave stabilized output voltages of +15 and -15V. These were used to operate the D.A.M.'s and to provide the 15 V applied to the R_1R_2 potentiometers.

Thus the generator, differential amplifier and driver current amplifier formed an automatic control circuit for controlling the speed of the associated motor and the two separate circuits driving the two chopper motors were identical in design. The chopper drive system under normal running conditions had a stability of about 1% over a period of 35 hours. However, to retain this stability, it was necessary at frequent intervals to clean all commutators and brushes and to tighten the flexible coupling between driving motor and generator.

III-52 Chopper reference signal circuit

Each chopper system provided the reference signal for the associated lock-in amplifier. The light from a small lamp L was chopped

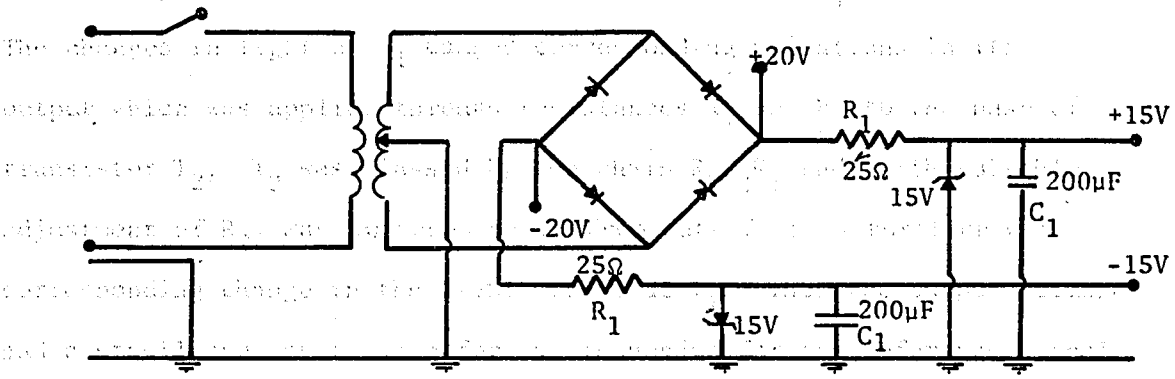

Figure (III-4): Power supply unit for chopper driver

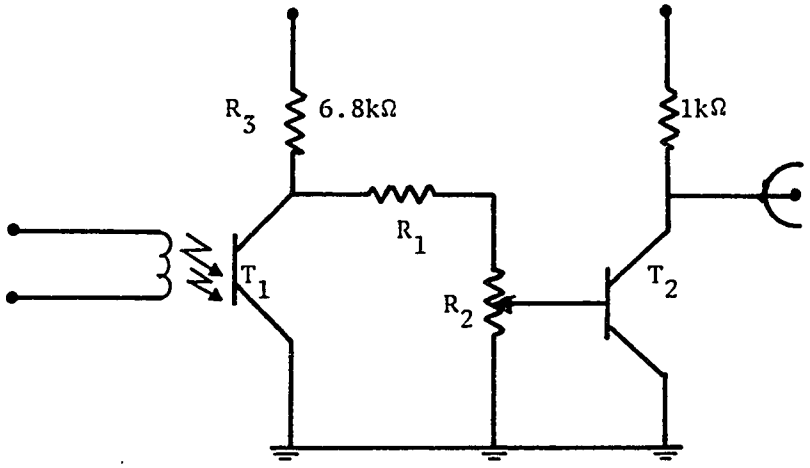

Figure (III-5): Reference circuit associated with the chopper driver

by the chopper blade and fell on a photo-transistor T_1 (Figure III-5). The changes in light on T_1 caused corresponding variations in its output which was applied through resistances R_1 and R_2 to the base of transistor T_2. T_2 was biassed by the chain $R_3R_2R_1$ and, with suitable adjustment of R_2, was switched by T_1 from cut-off to saturation with corresponding change in the light signal at T_1. Thus the output voltage had a stabilized square wave form as is needed for the reference signal to the lock-in amplifier and also satisfied the required conditions of being larger than and synchronous with the lock-in input signal.

CHAPTER IV

IV-1 PLASMA REFLECTION MEASURMENT

The reflectivity spectrum of a sample produced by the free carrier effect in a semiconductor is called the plasma reflection.

To eliminate the effect of fluctuations in the radiation source, temperature, amplification of the signal etc. which may occur when a single beam system is used and to improve the accuracy of the reflectivity measurement, the single beam operation of the monochromator was changed to double beam operation and the wavelength range of the monochromator extended. The basic design of this arrangement has been discussed in sections III-2, III-4 and III-5.

In the double beam operation, the monochromator was set up to be geometrically symmetrical, with similar mirrors and other identical instruments used simultaneously throughout the reflectivity measurement. The ratio of sample signal to reference signal was found by using a P.A.R. divider and this eliminated effects of atmospheric absorption and of any random source fluctuations which might occur during the measurement. The two beams, one chopped at 26 Hz and the other at 71 Hz were converted into voltage signals by a single pyroelectric detector, and these signals amplified simultaneously by a single preamplifier to eliminate any effects of the characteristic of the instrument.

The pyroelectric detector is an a.c. device, which detects temperature levels with a high response time and low noise at room temperature.

To increase the resolution of the measurement as much as possible, a narrow exit slit proportional to the wavelength was used in all measurements in the wavelength range 9 to 30 μm. The spectral range of the wavelength drum on the monochromator was scanned at a very slow rate to obtain higher signal-to-noise ratio (noise $\approx t^{-b}$ where t is the time of absorption in the detector and b is positive). The reflection of the sample was compared with that of an aluminum mirror with an assumed reflectance of 98.5% (62B).

The characteristics of the instrument were eliminated by a special arrangement to measure absolute reflectivity as follows: First of all, the sample M_8 (Figure III-1) was a semiconductor alloy sample of $GaAs_xSb_{1-x}$ or $Ga_{1-x}Al_xAs$, and the voltage signal V_s for the samle was compared with the voltage V_r for the reference mirror (M_9). The variation of the ratio $R_1 = V_s/V_r$ was obtained over the range 9 to 30 μm, the value of R_1 being recorded on the chart recorder. Keeping all optical paths and electrical instruments the same, the sample and the reference mirror were interchanged and the above measurements repeated giving the ratio $R_2 = V_{s'}/V_{r'}$. R_2 was recorded on the same chart as R_1. The absolute reflectance of the sample R was obtained as

$$R = \left(\frac{V_s}{V_r} \cdot \frac{V_{s'}}{V_{r'}}\right)^{\frac{1}{2}} R_{ref} \qquad \text{(IV-1)}$$

where R_{ref} is the absolute reflectance of the reference mirror. For most specimens, repeat runs of the reflectivity were made and an average of the values from equation (IV-1) taken as the absolute reflectivity of the specimen.

IV-2 CALIBRATION OF DOUBLE BEAM ARRANGEMENT

The wavelength of the Baird spectrometer in the range 9 to 30 μm was calibrated using absorption lines, the wavelength of which had been determined by Dowie (53D) using a KBr prism.

Several precaution were taken to obtain high absorption with as high a resolution as possible. The absorption data for each individual run were fed into a recorder. At each 1.00 reading of the wavelength control drum, a relay caused a mark to be made on the recorder paper, and this was used for calibrating the system. The calibration was performed in three steps in order to obtain a good number of accurate points for the calibration graph.

First of all, three bowls containing CH_3OH, H_2O and solid CO_2 respectively were put in a styrofoam box with open ends through which the radiation passed. This increased the vapour concentrations in the air through which the beam was passing and improved the measurement of the position of atmospheric and CH_3OH absorption lines up to 29 μm. Those values were used to draw a calibration graph. The calibration graph was tested in the double beam arrangement, using polystyrene film to give high absorption at 11.0, 13.2 and 14.29 μm and for the longer wavelength points, a $PtCl_4$ film was used. This film was prepared in the chemistry department of the University of Ottawa, and calibrated with a high resolution spectrometer giving absorption points at 23.90 and 28.90 microns. These were used to extend the calibration curve of Baird spectrometer. The results were fitted to the atmospheric absorption curve as is shown in the calibration graph (Figure IV-1). To reduce errors from

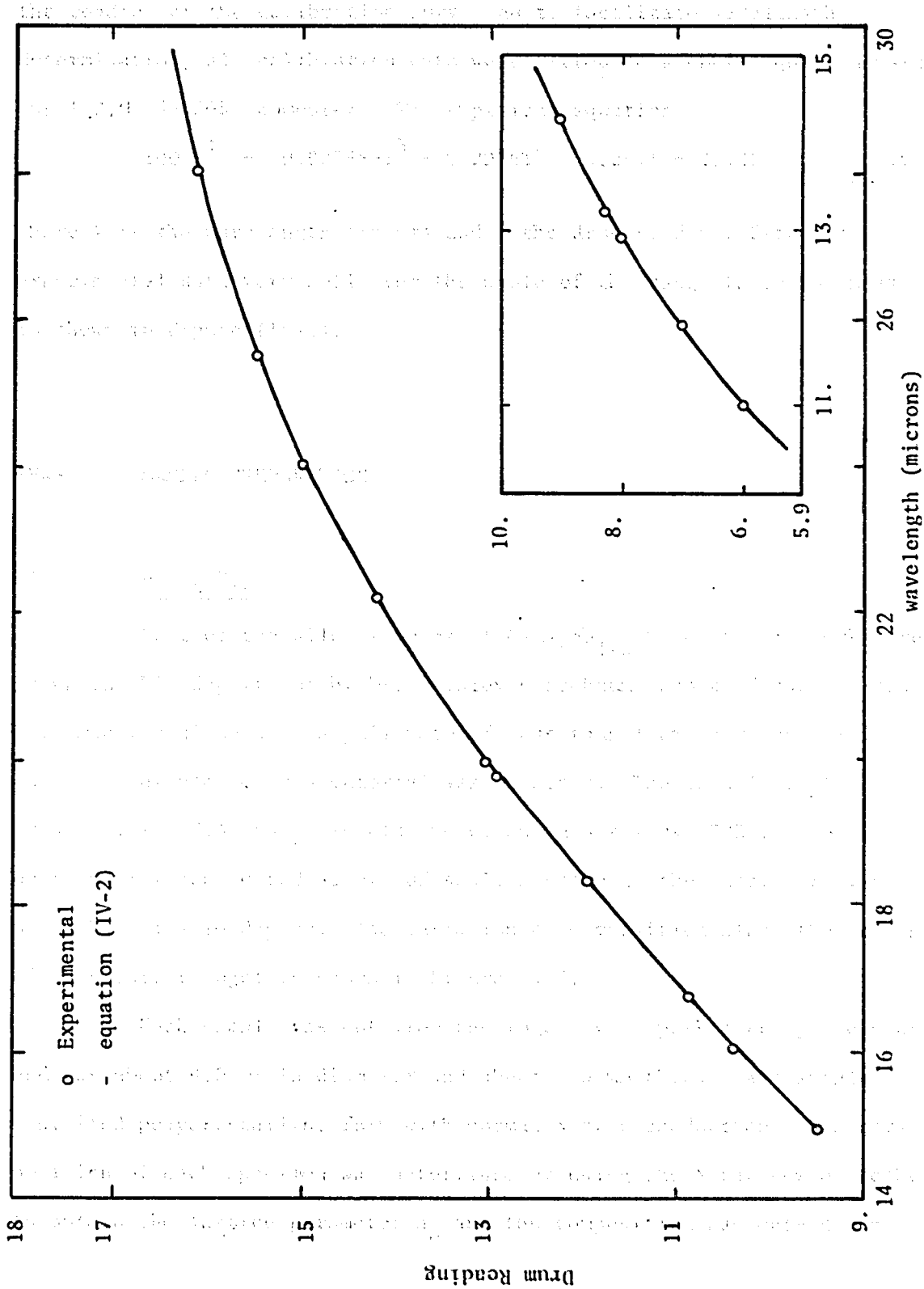

Figure (IV-1): Calibration curves in new arrangement

the reading of the calibration curve and to facilitate wavelength determination, all calibration data were fitted to a cubic equation using the I.B.M. 360/65 computer. The empirical equation

$$100\,\lambda^{-1} = 0.007588T^3 + 0.2976T^2 - 4.294T + 27.21 \qquad \text{(IV-2)}.$$

where λ is the wavelength (in μm) and T the drum reading, fitted the experimental data very well over the whole of the range 13 to 29 μm as is shown in Figure (IV-1).

IV-3 SAMPLE PREPARATION

a) $GaAs_xSb_{1-x}$

Most of the alloy samples of $GaAs_xSb_{1-x}$ used in this work were grown in this department by Dr. Stanley Rosenbaum, who used the horizontal Bridgman technique with a pull rate of less than 1 cm. per day. This ensured that homogeneous material was obtained. The details of the growth of the $GaAs_xSb_{1-x}$ ingots are given in his work (72R). He also particularly considered alloys of small x value in the ingot T.Z.F.-6 which had high Te doping. The variation of composition along the length of this latter ingot is shown in Figure IV-2.

Each sample was cut from the ingot by a spark cutting technique and was about 9.0 mm in diameter and about 1.0 mm thick. All samples exhibited polycrystalline form with normal N-type conduction. The composition of each specimen was determined by using the X-ray powder method to obtain the lattice parameter a_o and the composition was obtained by

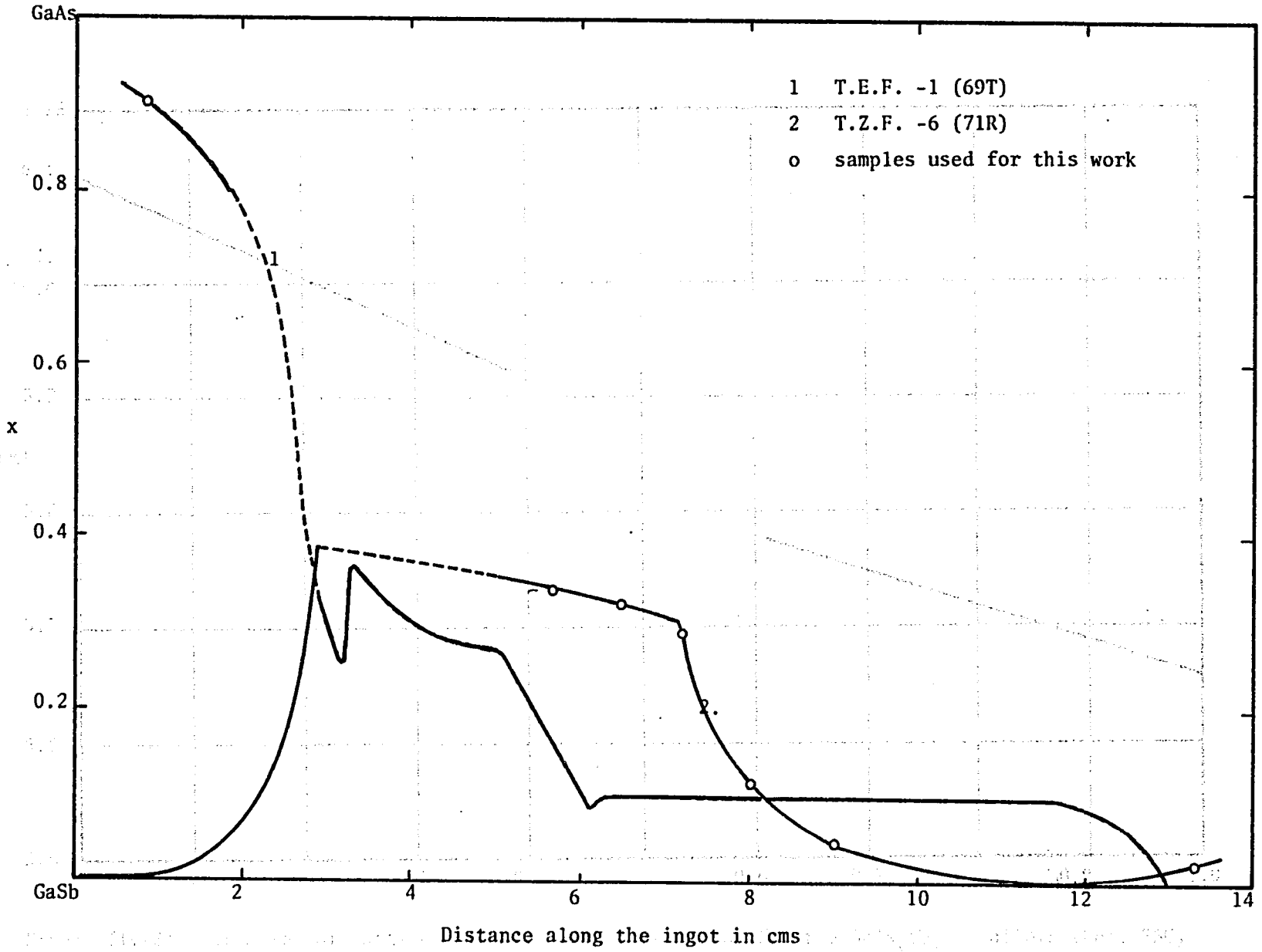

Figure (IV-2): Variation of composition along the length of the ingot for $GaAs_xSb_{1-x}$ alloys

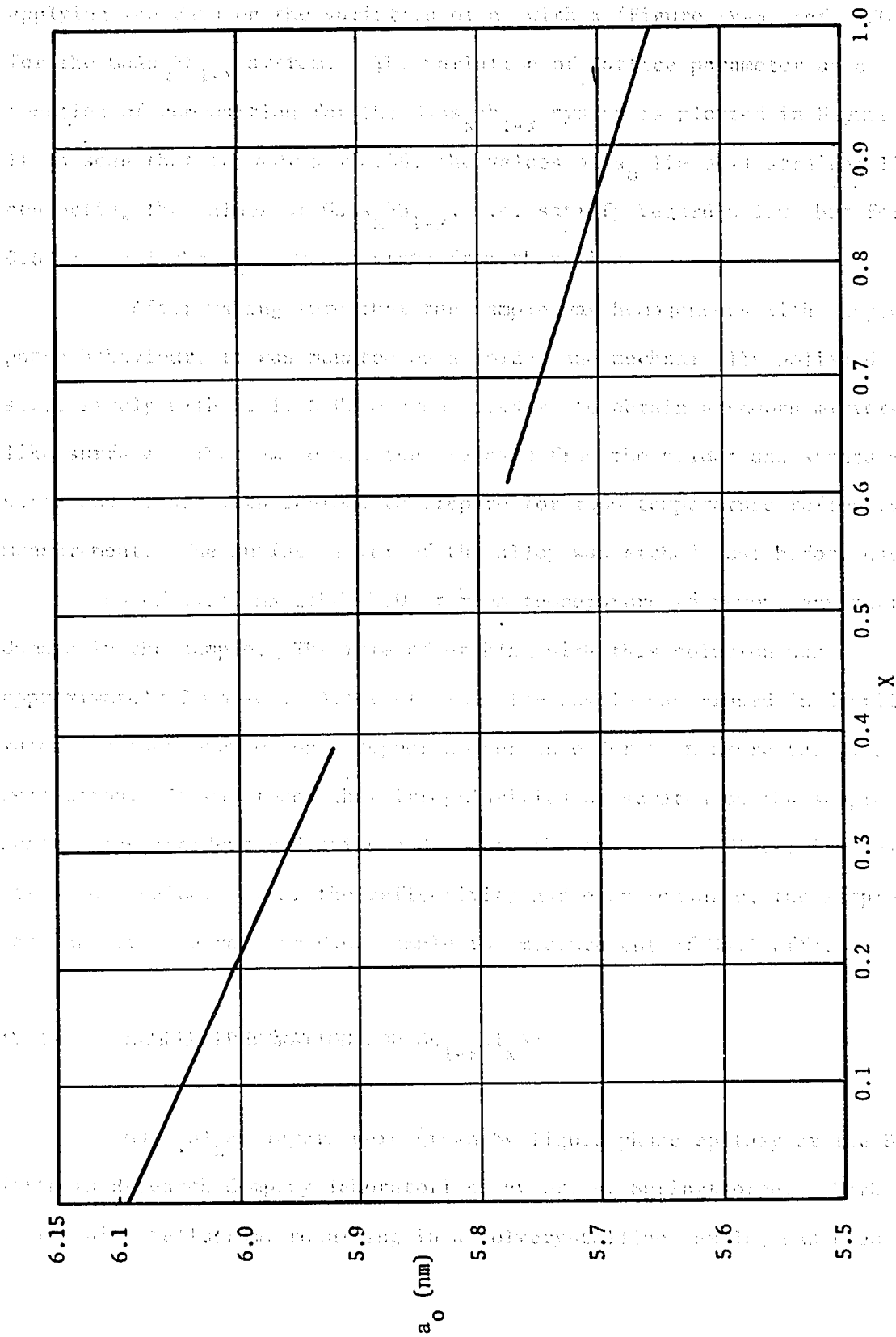

Figure (IV-3): Variation of lattice parameter with composition for the $GaAs_xSb_{1-x}$ alloys (Ref. 73G)

applying the data on the variation of a_o with x (Figure IV-3, ref. 73G) for the $GaAs_xSb_{1-x}$ system. The variation of lattice parameter as a function of composition for the $GaAs_xSb_{1-x}$ system is plotted in Figure IV-3. It is seen that for a $0 < x < 0.36$, the values of a_o lie on a straight line connecting the values at $GaAs_xSb_{1-x}$, i.e. satisfy Vegard's law, but for $0.61 < x < 1$ the a_o values deviate from that line.

After making sure that the sample was homogeneous with single phase behaviour, it was mounted on a holder and mechanically polished successively with 5, 1, 0.03 microns powders to obtain a smooth mirror-like surface. The sample was then removed from the holder and washed with water and rinsed with acetone to prepare for room temperature reflectivity measurement. The surface layer of the alloy was etched just before use in a solution of $1:2:2:HNO_3:HCl:H_2O$ at room temperature to remove any surface damage in the sample. The rate of etching with this solution was approximately 2 μm/sec. After etching, the sample was rinsed in distilled water and then mounted on a copper holder in order to measure the plasma reflection. It was found that irregularities or scratch on the sample scatter the incident radiation and reduce the measured reflectivity below its actual value. After the reflectivity had been measured, the sample was cut off as a van der Pauw sample for measurement of Hall effect.

IV-4 SAMPLE PREPARATION FOR $Ga_{1-x}Al_xAs$

$Ga_{1-x}Al_xAs$ layers were grown by liquid phase epitaxy at the Bell Northern Research Company laboratories, by Dr. A. Springthorpe. High doping with tellurium, resulting in a polycrystalline sample, was used to

obtain high carrier concentration for the reflectivity measurement. Ishii et al. have indicated (70I) that the distribution coefficient for Te in liquid phase-epitaxial growth of $Ga_{1-x}Al_xAs$ is independent of alloy composition. Details of the technical method of growth have been given by Springthorpe (74S).

The composition of the layers was determined at B.N.R.C. by quantitative electron microprobe analysis and by photoluminescence. The two measurements were in agreement within ±3%. Before the reflectivity measurements were taken, the alloy specimens were washed in acetone and then in concentrated HCl at 60°C for one second to remove any oxidation on the surface. In the case of the GaAs sample, the surface layer was etched at room temperature in a solution 2:2:1:H_2SO_4, H_2O_2, H_2O giving an etch rate of approximately 5 μm/sec. Immediately after etching, the sample was used for reflectivity measurement at room temperature.

IV-5 HALL EFFECT MEASUREMENT

Hall coefficients were measured by the van der Pauw method (58V) at room temperature, using the standard DC arrangement available in the physics department (Figure IV-4).

After the reflectivity measurement, the specimen was cut into a square van der Pauw sample. The contamination of the sample surface was removed by washing successively in acetone, trichoroethylene and de-ionized water. Gold-germanium was evaporated onto the four corners of the square specimen and the specimen annealed at 350°C in a He atmosphere

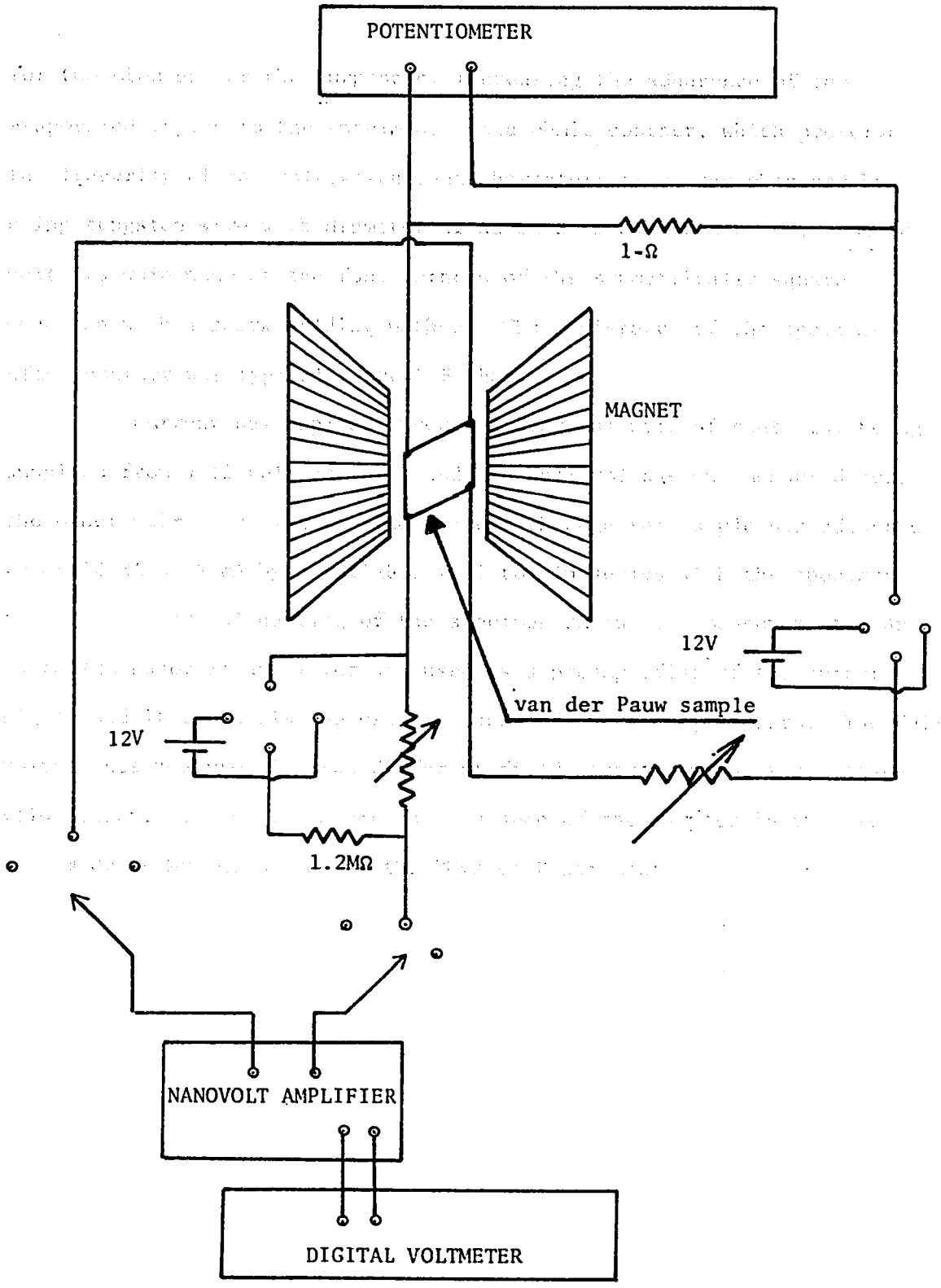

Figure (IV-4): Electrical Circuit for Hall effect measurements.

for two minutes for the purpose of increasing the adherence of the evaporated layers to the specimen. Good ohmic contact, which preserves the linearity of the voltage-current characteristics, was obtained by using tungsten wire with diameter of about 3 μm as a connector. Ohmic contacts were made at the four corners of the symmetrically square specimen with a spark welding method. The resistance of the specimen after contact was typically about 5 ohms.

Current was applied through a diagonal pair of contacts, being supplied from a 12 volt battery, and the Hall voltage was measured across the other pair of contacts. The current through the sample was adjusted to be 10 mA or 5 mA by a variable resistor in series with the specimen to avoid electrical heating of the specimen during the measurement. An Astrodata nanovolt amplifier was used as a preamplifier of the output signal and it could also be used to back-off the signal to zero. The Hall voltage was measured for two different field directions and the average value taken. The Hall measurements on some of the samples in this work were made by Mr. H. J. Lee of the Physics Department.

IV-6 VAN DER PAUW ANALYSIS AND EFFECT OF CONTACT SIZE

As indicated above, to determine the Hall coefficient by the van der Pauw method, current is applied on a pair of diagonal contacts of the square specimen and the Hall voltage was measured across the other pair. The Hall coefficient is then given as

$$R_H = \frac{d\Delta V}{Bi} \qquad \text{(II-4a)}$$

where d is the thickness of the specimen, i the current flowing and ΔV the change in measured voltage when the field B is applied. Usually, the field B is reversed and the average change in Hall voltage is used in equation IV-4a).

van der Pauw in his theoretical calculations (58V) assumed infinitesimally sized contacts to the sample, a condition which cannot be realized in practice. As was pointed out by Chwang (74C), the finite size of the contacts on a specimen has considerable effect on the potential distribution inside the sample and usually results in a reduction of the measured value of the Hall voltage from that for the ideal case. Hence, to determine the true Hall coefficient, the measured value must be multiplied by a correction factor. Chwang et al. (74C), calculated values of correction factor for both triangular and square contacts at the corners of a square sample. They found that the correction factor is a function of the $\Delta L/L$, which ΔL is the contact length and L the sample length, and the value of the Hall angle. Typical curves of correction factor against $\Delta L/L$ are shown in Figure IV-5.

In the present work, the contacts were approximately square in

shape and $\Delta L/L$ was taken as the average over the value at the four contacts. From the observed R_H values, an approximate value of Hall angle could be found and hence the required correction factor determined from the data of Chwang et al. The value of Hall coefficient and correction factor for the various samples measured in the present work are given in Table (V-1).

IV-7 ANALYSIS OF HALL COEFFICIENT DATA

For electrons in a single conduction band, the Hall coefficient is expressed as $R_H = \frac{r}{Ne}$ where N is the carrier concentration in the conduction band and r the Hall scattering factor which depends upon the scattering mechanisms. If the samples are highly degenerate (i.e. $E_f >> k_B T$) r = 1.0. But the samples used here were not within this limit. For the non-degenerate case r > 1.0 but it can be shown (59S) that for non-degenerate samples in infinite magnetic field r becomes unity, i.e.

$$R_\infty = \frac{1}{Ne} \qquad \text{(IV-4)}$$

Therefore, the value of R_H was determined as a function of B and extrapolated to infinite field, and R_∞ and hence N were determined

When two conduction bands overlap (labelled o for the band lower in energy and 1 for the second band), it can be shown that to a good approximation the low field Hall coefficient is given as

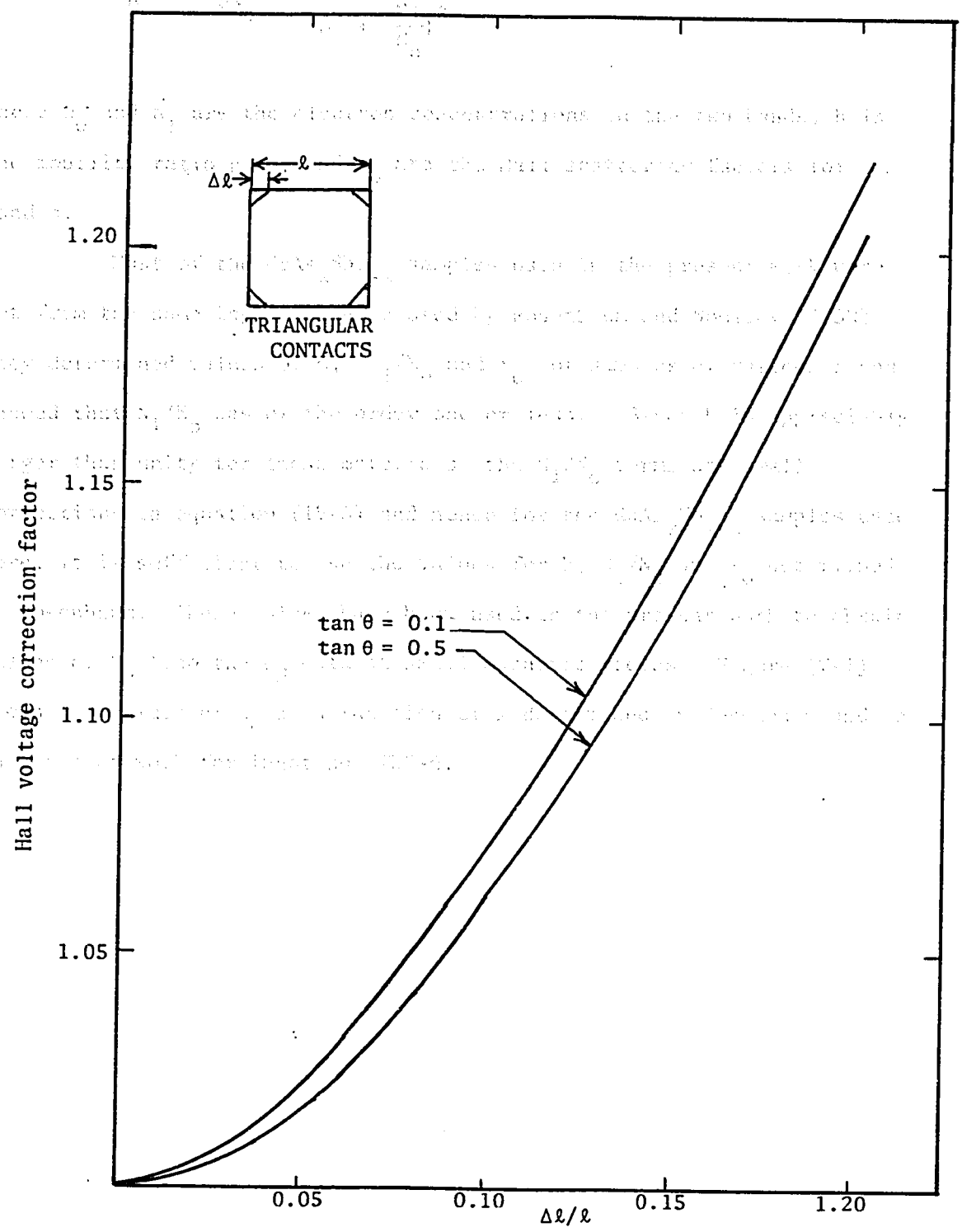

Figure (IV-5): Hall voltage correction factor vs. contact size for selected values of tan θ in van der Pauw measurements for triangular contacts (Ref. 74C).

$$R_H = \frac{r_o}{eN_o} \cdot \frac{(b^2 + \frac{N_1}{N_o})}{(b + \frac{N_1}{N_o})^2}$$

where N_o and N_1 are the electron concentrations in the two bands, b is the mobility ratio μ_o/μ_1 and r_o are the Hall scattering factors for band o.

Most of the $GaAs_xSb_{1-x}$ samples used in the present work were cut from the same ingot as those used by Rosenbaum and Woolley (75R). They determined values of b, N_1/N_o and r_o for samples of various x and showed that N_1/N_o was of the order one or less. Since b is appreciably larger than unity for these materials, the N_1/N_o terms are small corrections in equation (IV-5) and hence for the $GaAs_xSb_{1-x}$ samples used here, it is sufficient to use the values for b, N_1/N_o and r_o determined by Rosenbaum. These values have been used in the present work to obtain values of N_o from the R_H data at small magnetic fields. Figure (V-1) shows the values of N_o as a function of x determined by Rosenbaum and in the present work for ingot no. TZF-6.

V-1 METHOD OF ANALYSING EXPERIMENTAL DATA FOR SINGLE BAND (Γ_1) AND TWO CONDUCTION BAND (Γ_1 and L) SEMICONDUCTOR ALLOYS

Experimental data have been obtained from plasma reflection for alloys of the two systems $GaAs_xSb_{1-x}$ and $Al_xGa_{1-x}As$ in order to calculate values of effective mass, Fermi energy and dielectric constant. The method of analysis used here is based on that used by Thomas (69T) but has been modified to allow calculation of effective mass values in the case of a conduction band with electrons in two different minima (e.g. Γ_1 and L in $GaAs_xSb_{1-x}$). We shall discuss the procedure for the analysis of data for the single band ($Al_xGa_{1-x}As$) and two band ($GaAs_xSb_{1-x}$) cases in the general degeneracy condition.

For all alloys considered in the present work, the lowest minimum of the conduction band is located at the centre (Γ) of the Brillouin zone. It will be assumed that the condition $\omega\tau >> 1$ is satisfied in the infra-red range and under this condition, for wavelengths less than the plasma minimum, the imaginary part of the dielectric constant is small and the extinction coefficient is negligible compared with the index of refraction. Hence equation (II-37) simplifies to

$$\varepsilon = \eta^2 = \left(\frac{1 - \sqrt{R}}{1 + \sqrt{R}}\right) \qquad \text{(V-1)}$$

V-2 CASE OF GENERAL DEGENERACY

For $\lambda < \lambda_{min}$, the simplest form of expression for the dielectric constant which includes contributions of the lattice vibrations has been chosen. The expression for dielectric constant in the range of interest of the measurements is

$$\varepsilon = \varepsilon_\infty \left(1 - \frac{\omega_p^2}{\omega(\omega + i\gamma)} + \frac{\Delta\varepsilon\, \omega_t^2}{\omega_t^2 - \omega^2 - i\gamma\omega}\right) = \varepsilon_\infty + \varepsilon_{FC} + \varepsilon_{LV} \tag{V-2}$$

In this equation, ε_∞ is the high frequency dielectric constant, i.e. the value in the absence of free carrier contribution or that obtained by extrapolation to zero wavelength. The second term in equn. (V-2) is due to the contribution of free carriers to the dielectric constant. This term, which is proportional to the refractive index, is due to absorption and emission by the free carriers and is thus dependent on the carrier concentration. For n-type semiconductors, when $\omega^2\tau^2 >> 1$ the damping factor γ is negligible and hence we have

$$\varepsilon_{FC} = \frac{\varepsilon_\infty\, \omega_p^2}{\omega^2} \tag{V-3}$$

where ω is the pulsatance of the incident radiation and ω_p is the electron plasma pulsatance which for a single band semiconductor is given by

$$\omega_p^2 = \frac{4\pi^2 n_o e^2}{m^* \varepsilon_o} \tag{V-4}$$

where n_o is the electron concentration and m* the electron effective mass.

For the two band semiconductor materials considered in this work, the lowest conduction band is at k = 0 (Γ point) and a set of equivalent minima at the L points are a little higher in energy. At room temperature, there will be electrons in both bands and the value of ε_{FC} will be taken as the sum of the contributions from the two types of carriers, i.e. equations (V-3) and (V-4) then give

$$\varepsilon_{FC} = \left(\frac{n_o}{m_o^*} + \frac{n_1}{m_1^*}\right) \frac{e^2\lambda^2}{4\pi^2 c^2 \varepsilon_o} \qquad \text{(V-5)}$$

where n_o and n_1 are the carrier concentrations and m_o^* and m_1^* the effective masses of electrons in the (000) and <111> bands respectively. Equn. (V-5) can be written as

$$\varepsilon_{FC} = S_{FC}\left(1 + \frac{n_1}{n_o}\,\frac{m_o^*}{m_1^*}\right)\lambda^2 \qquad \text{(V-6)}$$

where

$$S_{FC} = \frac{e^2 n_o}{4\pi^2 c^2 \varepsilon_o m_o^*} \qquad \text{(V-7)}$$

and the value of m_o^*/m_1^* may be taken as 9 (72B) to the accuracy required in the correction term in equn. (V-6).

The third term in equn. (V-2) gives the contribution of lattice vibrations to the dielectric constant, which is

$$\varepsilon_{LV} = \frac{\Delta\varepsilon\ \omega_t^2}{\omega_t^2 - \omega^2 - i\gamma\omega} \qquad \text{(V-8)}$$

where ω_t and ω_ℓ are the transverse and longitudinal optical phonon pulsatance and $\Delta\varepsilon (= \varepsilon_s - \varepsilon_\infty)$ is the difference between the static and high

frequency dielectric constants which are related by the Lyddane-Fochs-Teller relation (41L).

$$\frac{\omega_\ell}{\omega_t} = \left(\frac{\varepsilon_s}{\varepsilon_\infty}\right)^{\frac{1}{2}} \qquad \text{(V-9)}$$

Assuming that ω_t and ω_ℓ are independent of carrier concentration, since the reflectively measurements are made at wavelengths shorter than that for reststrahlen effects, in this range $\omega^2 >> \omega_t^2$, γ^2 so that ω_t^2 and γ^2 are negligible and equn. (V-8) reduces to

$$\varepsilon_{LV} = S_{LV}\lambda^2 \qquad \text{(V-10)}$$

where

$$S_{LV} = \varepsilon_\infty(\nu_\ell^2 - \nu_t^2) \qquad \text{(V-11)}$$

and ν_ℓ and ν_t are the longitudinal and transverse optical phonon wave numbers. Thus equn. (V-2) for the dielectric constant of alloys of interest in the system $GaAs_xSb_{1-x}$ can be written

$$\varepsilon = \varepsilon_\infty - S_R\lambda^2 \qquad \text{(V-12)}$$

where

$$S_R = S_{FC}\left(1 - \frac{n_1}{n_2} \cdot \frac{m_o^*}{m_1^*}\right) - (\nu_\ell^2 - \nu_t^2) \qquad \text{(V-13)}$$

In the analysis of the experimental data, values of ε were determined from reflectivity values using equn. (V-1), and the shape of a graph of ε vs. λ^2 gave values of S_R. It was assumed that ν_ℓ and ν_t varied linearly with alloy composition and hence values of S_{FC} were obtained, n_o and n_1 being available from the electrical measurements as indicated in para(IV-7). For the case of $Al_xGa_{1-x}As$ alloys with a single

conduction band, n_1 is zero in equn. (V-13) and thus values of S_{FC} are obtained from the reflectivity data.

The value of ε from the theoretical calculation in Chapter II can be obtained from equn. (II-82) as

$$\varepsilon = \varepsilon_\infty - \left(\frac{e^2}{12\pi^4 c^2 \hbar^2 \varepsilon_o}\right) \lambda^2 \int k^2 \nabla_k E \nabla_k f_o \, dE + \varepsilon_{LV} \qquad \text{(V-14)}$$

and from the Kane model (equn. II-13)

$$\nabla_k E = 2ak^2 \left[1 + \left\{1 + \frac{4a}{E_o^*}\left(\frac{m}{m_{oo}^*} - 1\right) k^2\right\}^{\frac{1}{2}} \left(\frac{m}{m_{oo}^*} - 1\right)\right] \qquad \text{(V-15)}$$

where $a = \hbar^2/2m$ and the first term ak^2 can be neglected in comparison with the other terms. Rearrangement of the Kane equation gives k in terms of E as

$$k = \left\{\frac{E(E + E_o^*)}{aE_o^*\left(\frac{m}{m_{oo}^*} - 1\right)}\right\}^{\frac{1}{2}} \qquad \text{(V-16)}$$

Substituting first for $\nabla_k E$ and then for k in equn (V-15) and then comparing with equn (V-12) gives

$$S_{FC} = e/\left[6k_B T \, a^{\frac{1}{2}} \pi^4 c^2 \hbar^2 \varepsilon_o \left\{E_o^* \left(\frac{m}{m_{oo}^*} - 1\right)\right\}^{3/2}\right]$$

$$\times \int \frac{E(E + E_o^*)^{3/2}\left[1 + \left(\frac{m}{m_{oo}^*} - 1\right)\left\{1 + \frac{4E}{E_o^*}(E + E_o^*)\right\}^{-\frac{1}{2}}\right]}{2 + \exp\left(\frac{E - E_F}{k_B T}\right) + \exp\left(\frac{E_F - E}{k_B T}\right)} \qquad \text{(V-17)}$$

where k_B is Boltzmann's constant.

By substituting equns. (II-84) and (V-17) into equn (II-87) and integrating over energy, an expression for the carrier concentration in the Γ band is obtained as

$$n_o = \frac{1}{3\pi^2 k_B T \{aE_o^* (\frac{m}{m_{oo}^*} - 1)^{3/2}\}} \int_o^\infty \frac{\{E(E + E_o^*)\}^{3/2} dE}{2 + \exp(\frac{E - E_F}{k_B T}) + \exp(\frac{E_F - E}{k_B T})} \qquad \text{(V-18)}$$

Since n_o and S_{FC} have been determined experimentally the only unknown parameters in equns. V-17 and V-18 are E_F, m_{oo}^* and E_o^*. In previous work on similar alloys (69V), a satisfactory expression for $E_o^*(T)$ has been found to be

$$\frac{E_o(O) + E_o(T)}{2} \qquad \text{(V-19)}$$

and so this expression will be used here. Then simultaneous solution of the two equations gives values for m_{oo}^* and E_F. Using a iterative, numerical integration method on the IBM 360/65 computer, values of m_{oo}^* were obtained from each equation for a series of values of E_F. The programme then searched for the value of E_F which gave identical values of m_{oo}^* from both equations, these m_{oo}^* and E_F values being the solution required. Alternatively graphs of m_{oo}^* versus E_F could be plotted and the values at the point of intersection determined.

V-3 DEGENERATE CASE

In a semiconductor material with large carrier concentration, usually $E_f >> k_B T$ and this material is said to be degenerate. In this condition, if $\omega_p \tau >> 1$, there is a sharp absorption in the infrared at the plasma edge and this affects the value of refractive index. Furthermore, as shown in equn. (II-49), if the extinction coefficient κ is negligible compared with refractive index η, when η approaches unity, the reflectivity R approaches zero, the corresponding wavelength being called λ_{min}. As the wavelength is further increased, the reflectivity rises very sharply to a maximum value. In such a case, the result can be expressed by equn. (II-49) in the form

$$\left(\frac{m^*_f}{m}\right) = \frac{N_o e^2}{4\pi^2 c^2 m \varepsilon_o (\varepsilon_\infty - 1)} \lambda^2_{min} \qquad \text{(V-20)}$$

where m^*_f/m is the effective mass at the Fermi level. If N_o and ε_∞ are known, m^*_f/m can easily be determined. This method has been used for determining effective mass values in GaAs (59S). In the present work, heavily doped samples were not available and therefore the condition of degeneracy did not apply. Further the minimum reflectivity was not close to zero and the analysis for the condition of general degeneracy described above had to be used.

Another method of analysing the reflectivity measurement to obtain an effective mass value has been proporsed by Lyden (64L), for the case when the reflectivity measurement shows a pronounced minimum. The Lyden analysis gives a cubic equation in (m*/m) which can be solved

if the dielectric constant is known and initial estimates for the average relaxation time τ are made from mobility measurements. Riedl (67R) proposed another method for a graphical fitting of R as a function of λ, which leans heavily on the position of the minimum but, by making use of the whole curve, allows the average relaxation time to be determined independently. This method was used by Dionne (71D) to calculate effective mass values from reflectivity measurements on lead-tin telluride alloys.

V-4 DATA, RESULTS AND DISCUSSION

As indicated in section III-1, the monochromator, modified to double beam arrangement and with the wavelength range extended, was used to measure plasma reflection at room temperature. The monochromator was calibrated by observation of the absorption lines of water vapour, CO_2, CH_3OH, $PtCl_4$ and polystyrene film in the wavelength range 9 to 30 μm. The values of wavelength against monochromator drum reading in the new arrangement are given in Figure (IV-2). The data were fitted by I.B.M. computer to a cubic equation in T of the form

$$100\lambda^{-1} = 0.007588T^3 + 0.3976T^2 - 4.294T + 27.2 \qquad \text{(V-21)}$$

It was found that equation (V-21) is a good fit to the experimental data.

V-42 $GaAs_xSb_{1-x}$ Alloys

The infrared reflectivity and Hall effect measurements were made at room temperature on nine samples of the alloys $GaAs_xSb_{1-x}$. Some part of each alloy sample was used for X-ray powder photograph to give values of lattice parameter and hence of mole fraction x.

The Hall coefficients of the van der Pauw samples were corrected for contact size as described in section IV-6 and hence values of N_o determined as shown in section IV-7, using the values of r_o, b and N_1/N_o given by Rosenbaum and Woolley (75R) for the appropriate value of x. The resulting values of N_o together with the correction factors for the van der Pauw samples are given in Table (V-1) and the variation of N_o as a function of composition x is shown in Figure (V-1).

From the infrared reflectivity measurements for values of wavelength less than that of the plasma minimum, values of η^2 were determined from equation (II-41) and graphs of η^2 against λ^2 were plotted, some typical results being shown in Figures (V-2) and (V-3). All the graphs were found to be linear as predicted by equation (V-12). The intercept of η^2 at the zero wavelength gives the optical dielectrical constant ε_∞ and the variation of ε_∞ with composition x is shown in Figure (V-4). There was some scatter in these points and thus it is not clear exactly how ε_∞ varies with x. It has been pointed out, that the disorder properties in semiconductor alloys cause changes in the density of states (73Y), effective mass (73W, 74P), energy gap (73S) and electronic state (75K) and all these quantities contribute to the optical properties observed in the reflectivity measurement. Thus some changes in ε_∞ due

Table (V-1) TYPICAL HALL DATA FOR $GaSb_{1-x}As_x$ AND $Ga_{1-x}Al_xAs$.

Ingot	Composition x	Thickness ℓ (mm)	Carrier Concentration N_o $(10^{24}/m^3)$	Correction Factor
T.Z.F. -6	0.03	0.325	0.7875	1.12
T.Z.F. -6	0.04	0.683	0.7632	1.14
T.Z.F. -6	0.11	0.385	1.035	1.14
T.Z.F. -5	0.17	0.48	0.370	1.13
T.Z.F. -6	0.298	0.50	2.128	1.1
T.Z.F. -6	0.33	0.383	2.238	1.1
T.Z.F. -6	0.34	0.383	2.95	1.15
T.Z.F. -1	0.90	0.523	1.016	1.11
GaAs		0.325	2.939	1.12
$Ga_{1-x}Al_xAs$	0.106	0.065	1.552	1.006
$Ga_{1-x}Al_xAs$	0.13	0.055	1.238	1.005

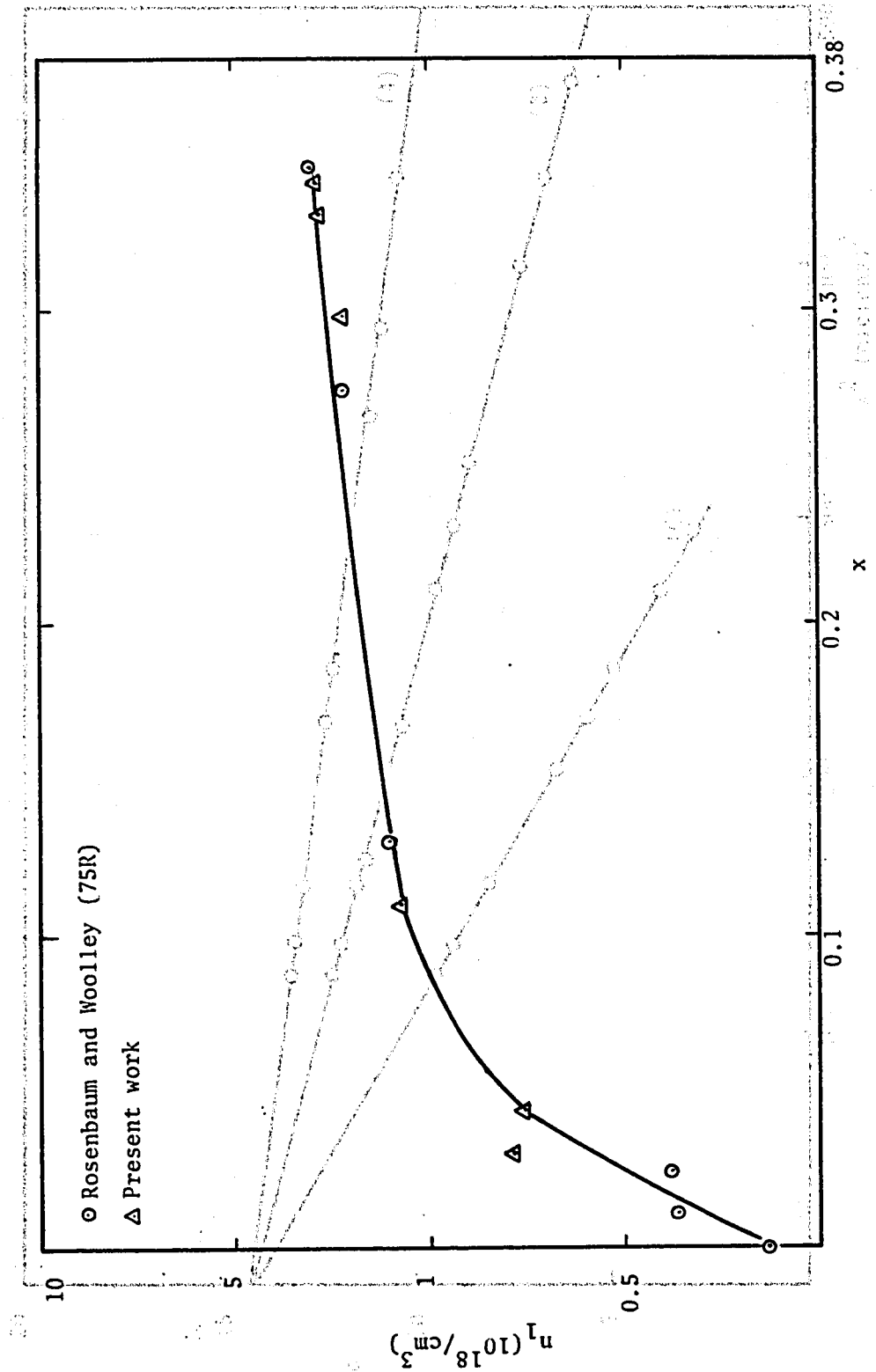

Figure (V-1): Variation of the carrier concentration with composition in the $GaAs_xSb_{1-x}$ alloys for the ingot T.Z.F. -6.

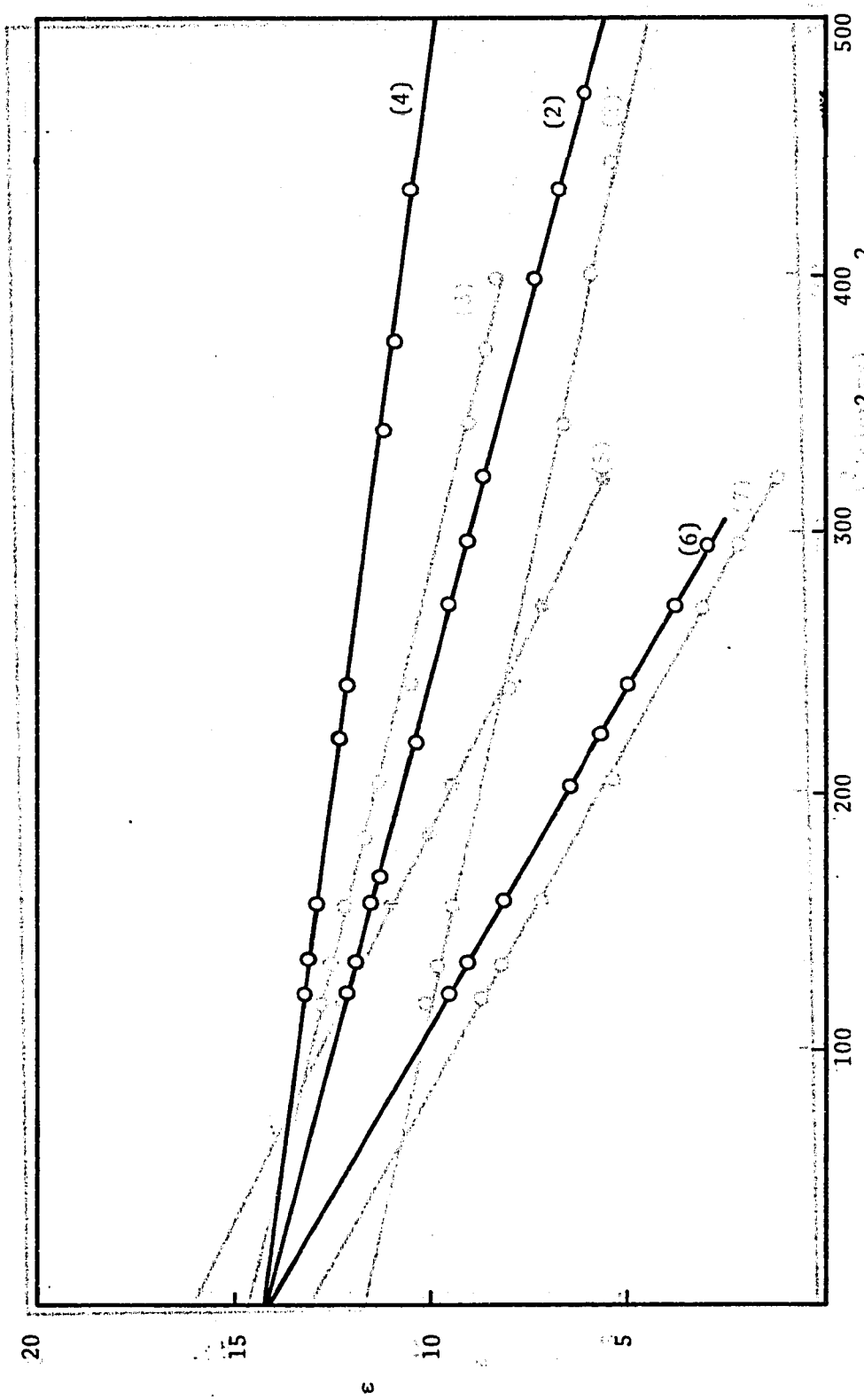

Figure (V-2): Typical graphs of ε vs. λ^2 for $GaAs_xSb_{1-x}$ alloys

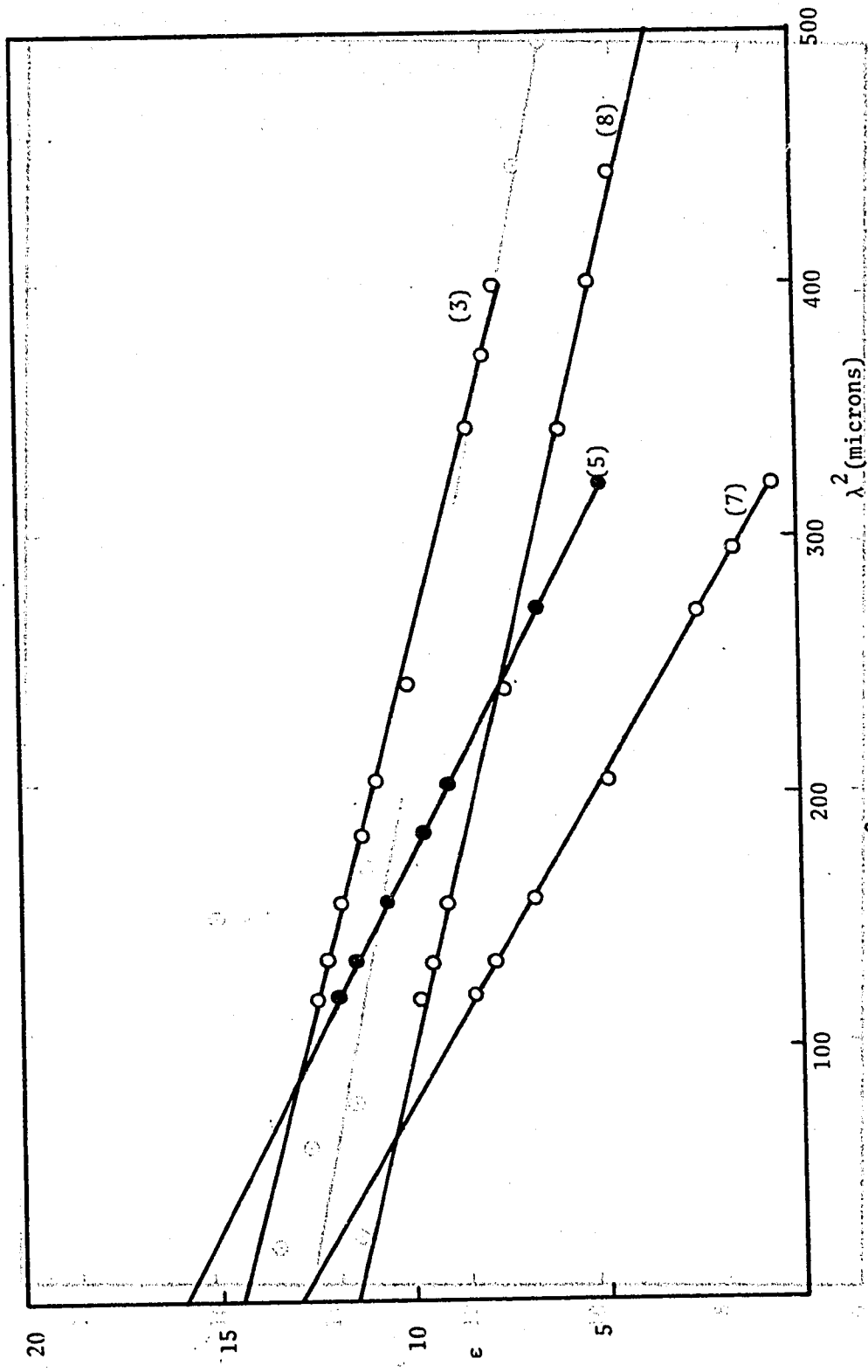

Figure (V-3): Typical graphs of ε vs. λ^2 for $GaSb_{1-x}As_x$

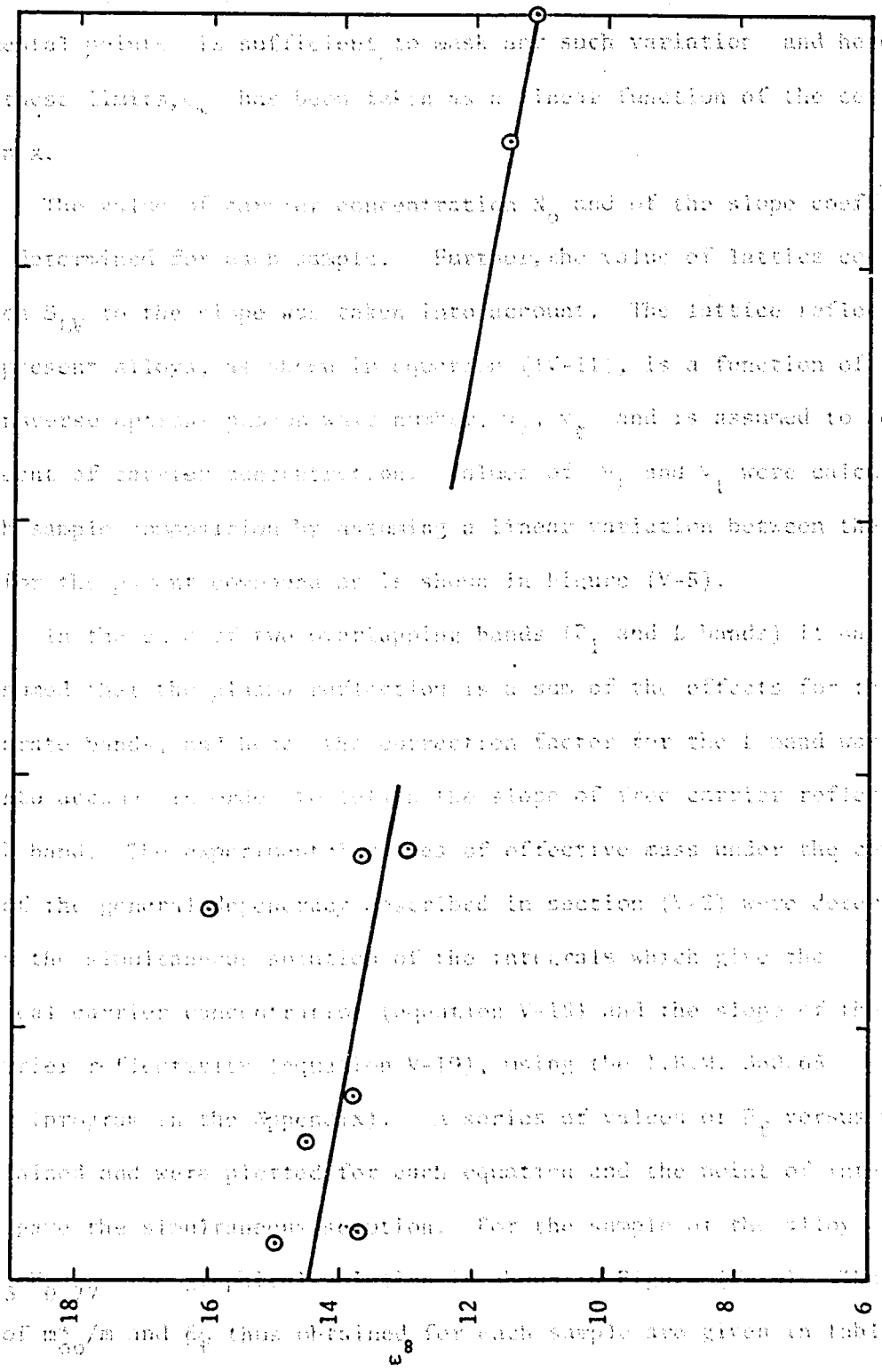

Figure (V-4): Variation of ε_∞ with composition for $GaAs_xSb_{1-x}$.

to disorder might be expected to occur. However, the random error in the experimental points is sufficient to mask any such variation and hence, within these limits, ε_∞ has been taken as a linear function of the composition x.

The value of carrier concentration N_o and of the slope coefficient S_{FC} was determined for each sample. Further, the value of lattice contribution S_{LV} to the slope was taken into account. The lattice reflection in the present alloys, as shown in equation (IV-11), is a function of longitudinal and transverse optical phonon wave number, ν_ℓ, ν_t and is assumed to be independent of carrier concentration. Values of ν_ℓ and ν_t were calculated for each sample composition by assuming a linear variation between the values for the parent compound as is shown in Figure (V-5).

In the case of two overlapping bands (Γ_1 and L bands) it has been assumed that the plasma reflection is a sum of the effects for the two separate bands, and hence the correction factor for the L band was taken into account in order to obtain the slope of free carrier reflectivity of the Γ band. The experimental values of effective mass under the condition of the general degeneracy described in section (V-2) were determined by the simultaneous solution of the integrals which give the statistical carrier concentration (equation V-18) and the slope of the free carrier reflectivity (equation V-19), using the I.B.M. 360/65 computer (program in the Appendix). A series of values of E_f versus m^*_{oo}/m were obtained and were plotted for each equation and the point of intersection gave the simultaneous solution. For the sample of the alloy $GaAs_{0.33}Sb_{0.77}$ the graphical solution is shown in Figure (V- 6). The values of m^*_{oo}/m and E_f thus obtained for each sample are given in table(V-2) and

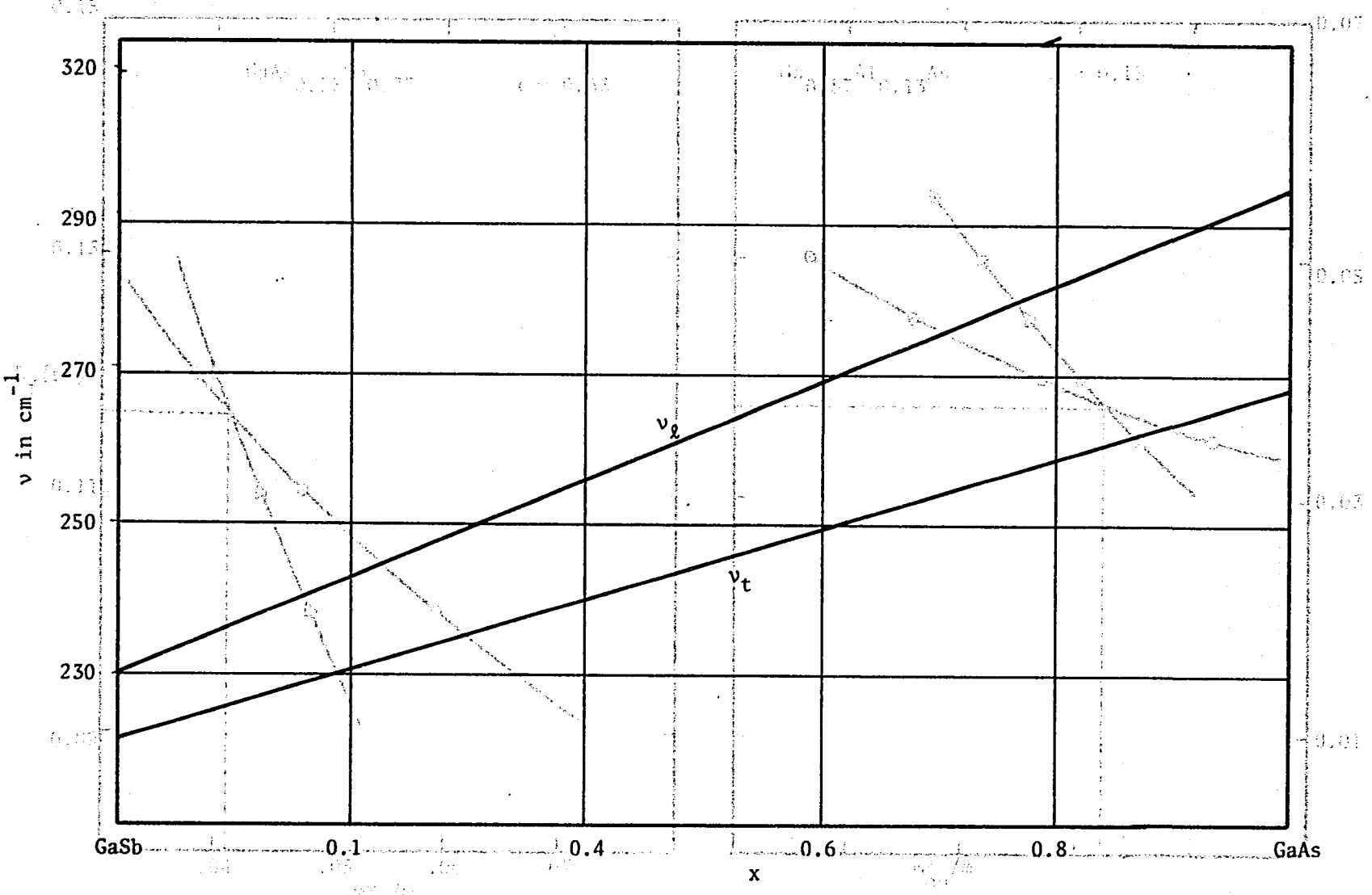

Figure (V-5): Variation of longitudinal and transverse optical phonon frequencies for $GaAs_xSb_{1-x}$ alloys according to reference (72R) and (68B).

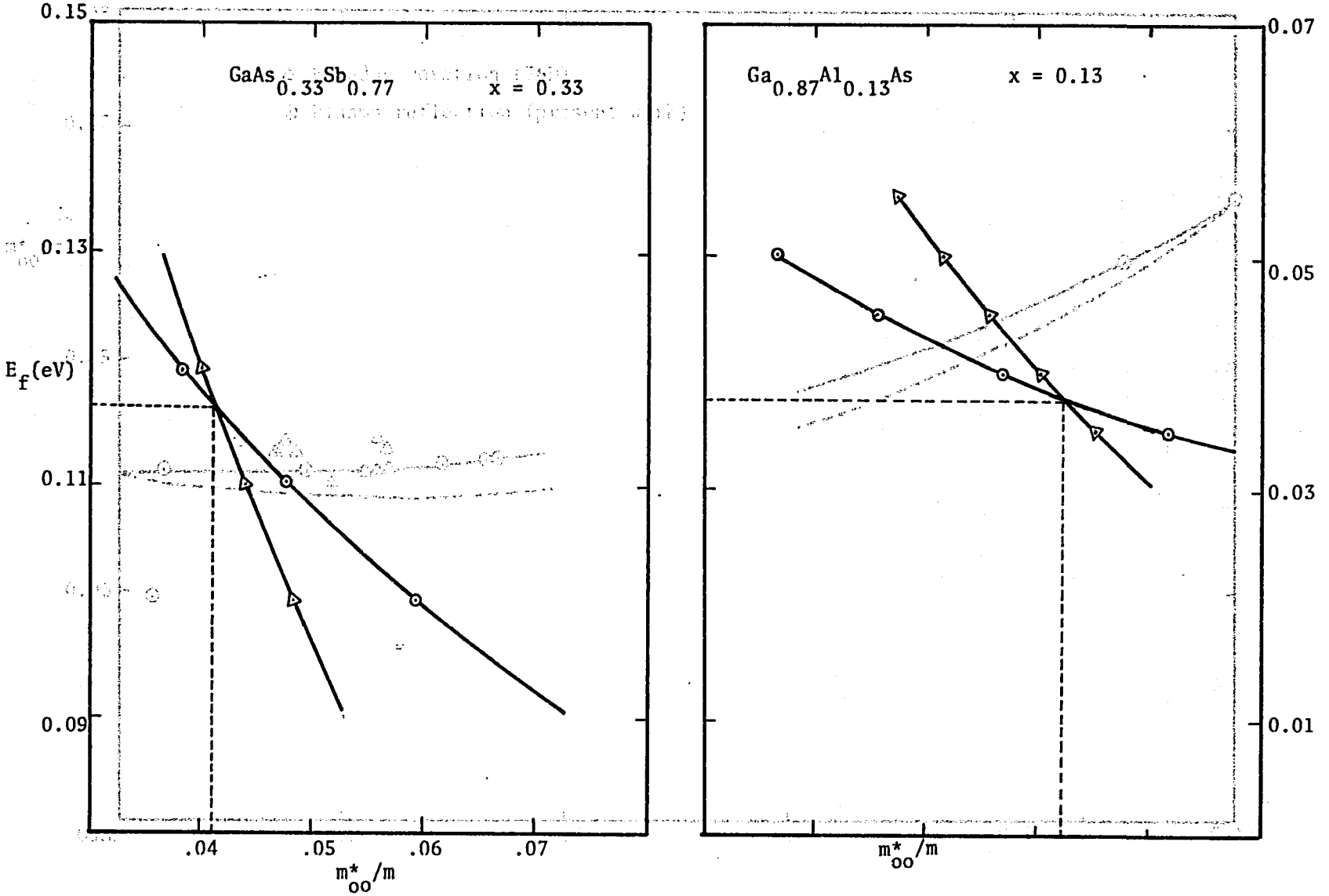

Figure (V-6): Graphical solution of the equation (V-18) and (V-19) to obtain m^*_{oo}/m and E_f for two typical sample $GaAs_xSb_{1-x}$ and $Ga_{1-x}Al_xAs$.

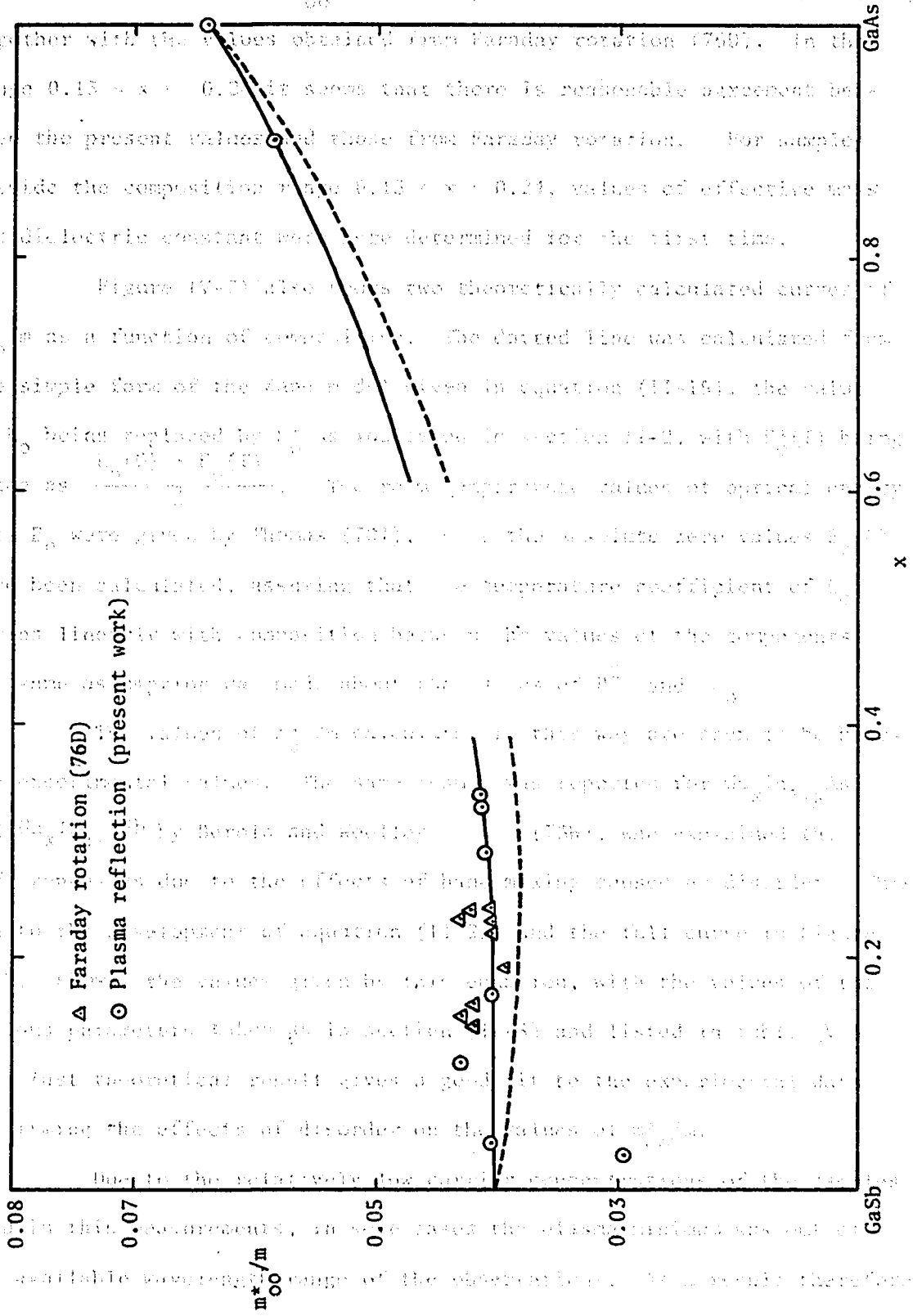

Figure (V-7): Variation of m^*_o/m with composition for $GaAs_xSb_{1-x}$.

(V-3). The variation of m^*_{oo}/m with composition x is shown in Figure (V-7) together with the values obtained from Faraday rotation (76D). In the range $0.13 < x < 0.24$ it seems that there is reasonable agreement between the present values and those from Faraday rotation. For samples outside the composition range $0.13 < x < 0.24$, values of effective mass and dielectric constant were here determined for the first time.

Figure (V-7) also shows two theoretically calculated curves of m^*_{oo}/m as a function of composition. The dotted line was calculated from the simple form of the Kane model given in equation (II-15), the value of E_o being replaced by E^*_o as indicated in section II-2, with $E^*_o(T)$ being taken as $\frac{E_o(0) + E_o(T)}{2}$. The room temperature values of optical energy gaps E_o were given by Thomas (70T), while the absolute zero values $E_o(0)$ have been calculated, assuming that the temperature coefficient of E_o varies linearly with composition between the values of the components. The same assumption was made about the values of P^2 and Δ_o.

The values of m^*_{oo}/m calculated in this way are seen to be below the experimental values. The same result was reported for $Ga_xIn_{1-x}As$ and $Ga_xIn_{1-x}Sb$ by Berolo and Woolley (73W), who explained the differences as due to the effects of band mixing caused by disorder. This led to the development of equation (II-25) and the full curve in Figure (V-7) shows the values given by this equation, with the values of the various parameters taken as in section (II-5) and listed in table (V-5). This last theoretical result gives a good fit to the experimental data confirming the effects of disorder on the values of m^*_{oo}/m.

Due to the relatively low carrier concentrations of the samples used in this measurements, in some cases the plasma minimum was out of the available wavelength range of the observations. As a result therefore,

Table (V-2) EXPERIMENTAL DATA FOR $GaSb_{1-x}As_x$.

Ingot	Code No. of Specimen	Composition x	Lattice Parameter a_o (nm)	ε_∞
T.Z.F. -6	1	0.03	0.6071	15
T.Z.F. -6	2	0.04	0.6068	13.7
T.Z.F. -6	3	0.11	0.6047	14.5
T.Z.F. -5	4	0.17	0.6020	13.8
T.Z.F. -6	5	0.298	0.5965	16.0
T.Z.F. -6	6	0.33	0.5949	13.7
T.Z.F. -6	7	0.34	0.5943	13.0
T.Z.F. -1	8	0.90	0.5687	11.5

Table (V-3) EXPERIMENTAL DATA FOR $GaSb_{1-x}As_x$

Code No. of Specimen	N_o 10^{24}	m_o^*/m	E_f (eV)	S_{LV} $(10^{-2}m^{-2})$	S_{FC} $(10^{-2}m^2)$
1	0.7875	0.0293			
2	0.7632	0.0402	0.0527	0.068	1.332
3	1.035	0.0430	0.0632	0.076	1.682
4	0.370	0.0403	0.0235	0.081	0.688
5	2.128	0.0407	0.1181	0.071	3.374
6	2.237	0.0411	0.1172	0.103	3.572
7	2.295	0.0414	0.118	0.095	3.665
8	1.016	0.0587	0.0432	0.159	0.1381

Table (V-4) COMPUTED VALUES FROM PLASMA MINIMUM FOR $GaSb_{1-x}As_x$.

Code No. of Specimen	λ_{min}	κ_{min}	τ 10^{-13} sec	ω_p 10^{14}/sec	μ (m^2/volt.sec)	σ ($10^5 \Omega^{-1} m^{-1}$)
1	24.09	0.138	2.898	0.686	0.173	1.912
2	27.31	0.044	15.651	0.648	0.685	7.110
3	25.01	0.144	2.649	0.653	0.108	1.131
4	39.43	0.016	76.987	0.456	3.359	23.56
5	17.89	0.187	1.254	0.873	0.054	0.758
6	16.13	0.097	3.006	1.096	0.128	2.258
7	15.54	0.008	5.981	1.117	2.543	45.509
8	26.01	0.073	6.398	1.076	0.192	2.022

Table (V-5): PARAMETER USED IN EQUATION (II-25)

x	E_o (eV)	E_o^* (eV)	Δ_o (eV)	$E_o^*+\Delta_o$ (eV)	m_{co}/m	m_c/m
0	0.72	0.77	0.86	1.63	0.040	0.040
0.1	0.70	0.75	0.81	1.56	0.039	0.040
0.2	0.68	0.73	0.76	1.49	0.038	0.040
0.3	0.69	0.74	0.70	1.44	0.038	0.041
0.4	0.72	0.77	0.65	1.42	0.039	0.042
0.6	0.96	0.91	0.55	1.46	0.044	0.047
0.7	0.96	1.01	0.50	1.51	0.048	0.051
0.8	1.09	1.14	0.44	1.58	0.052	0.054
0.9	1.24	1.29	0.39	1.68	0.057	0.058
1.0	1.42	1.47	0.34	1.81	0.064	0.064

equation (V-20) has been used to give an approximate value for λ_{min} from the m^*_{oo}/m values determined in the general degeneracy case. These values have been used to calculate values of optical relaxation time τ, optical mobility, optical conductivity and extinction coefficient at the minimum reflectivity using equations (II-54) and (II-61). These values are listed in table (V-4).

V-43 $Ga_{1-x}Al_xAs$ alloys

Plasma reflectivity measurements were made on two alloy samples of $Ga_{1-x}Al_xAs$ and a GaAs sample at room temperature. The alloy samples used here were epitaxial layers grown at the Bell Northern Research (B.N.R.) Laboratories where their composition was determined. With these samples some multiple reflection occurred throughout the reflectivity measurement.

From the measured reflectivity data R, values of η^2 as a function of λ^2 for these alloys are plotted in Figure (V-8). Again, the intercept of η^2 at zero wavelength gives the value of optical dielectric constant ε_∞ and the values of ε_∞ for the two alloys $Ga_{1-x}Al_xAs$ and for the GaAs sample are listed in Table (V-6). The slope of η^2 vs. λ^2 for each sample was calculated and the simultaneous solution of equations (V-18) and (V-19) used as before to give values for m^*_{oo} and E_f, the graphs in the case of the x = 0.13 sample being shown in Fig. (V-6). The values of m^*_{oo}/m and E_f so obtained are given in Table (V-6).

Due to the relatively large electron effective mass of the Γ_1 band in these alloys, large carrier concentrations were required to obtain the effective mass values in the plasma reflection. Also a conduction

band cross-over occurs in these alloys at around x = 0.30 and hence in the range $0.15 < x < 0.45$, two or multiband behaviour is to be expected. Since for alloys with $x < 0.30$ subsidiary band parameters are not known, analysis of the reflection data could not be carried out as for the $GaAs_xSb_{1-x}$ alloys. As a result, the number of samples in which infrared reflectivity could be used were limited.

The straight line on graph (V-9) drawn through the experimental points, when extrapolated to x = 1 gives a value close to the value estimated for the Γ_1 band electron effective mass for AlAs as indicated by Rode (74R).

The values of effective mass, dielectric constant, optical relaxation time, optical conductivity and optical mobility for these alloys were calculated and the results are recorded in Table (V-6).

Table (V-6): EXPERIMENTAL DATA FOR $Ga_{1-x}Al_xAs$

Alloys	Composition x		S_{LV}	S_{FC}	λ_{min}	$\omega p / 10^{14}$	k_{min}
GaAs	-	11.10	0.162	3.538	16.12	1.076	0.0846
$Ga_{1-x}Al_xAs$	0.106	10.6	0.16	1.75	23.55	0.754	0.0244
$Ga_{1-x}Al_xAs$	0.13	11.75	0.164	1.38	25.00	0.707	0.0213

Alloys	Composition	η $10^{-24}/m^3$	m^*_{oo}/m	E_f eV	τ (10^{-13}sec)	μ (m^2/volt.sec)	σ ($x10^5$ -1_m-1)
GaAs	-	2.939	0.0641	0.037	0.2951	0.809	1.396
$Ga_{1-x}Al_xAs$	0.106	1.552	0.0718	0.0377	2.3484	5.752	6.951
$Ga_{1-x}Al_xAs$	0.13	1.238	0.0723	0.0478	1.5815	6.279	7.114

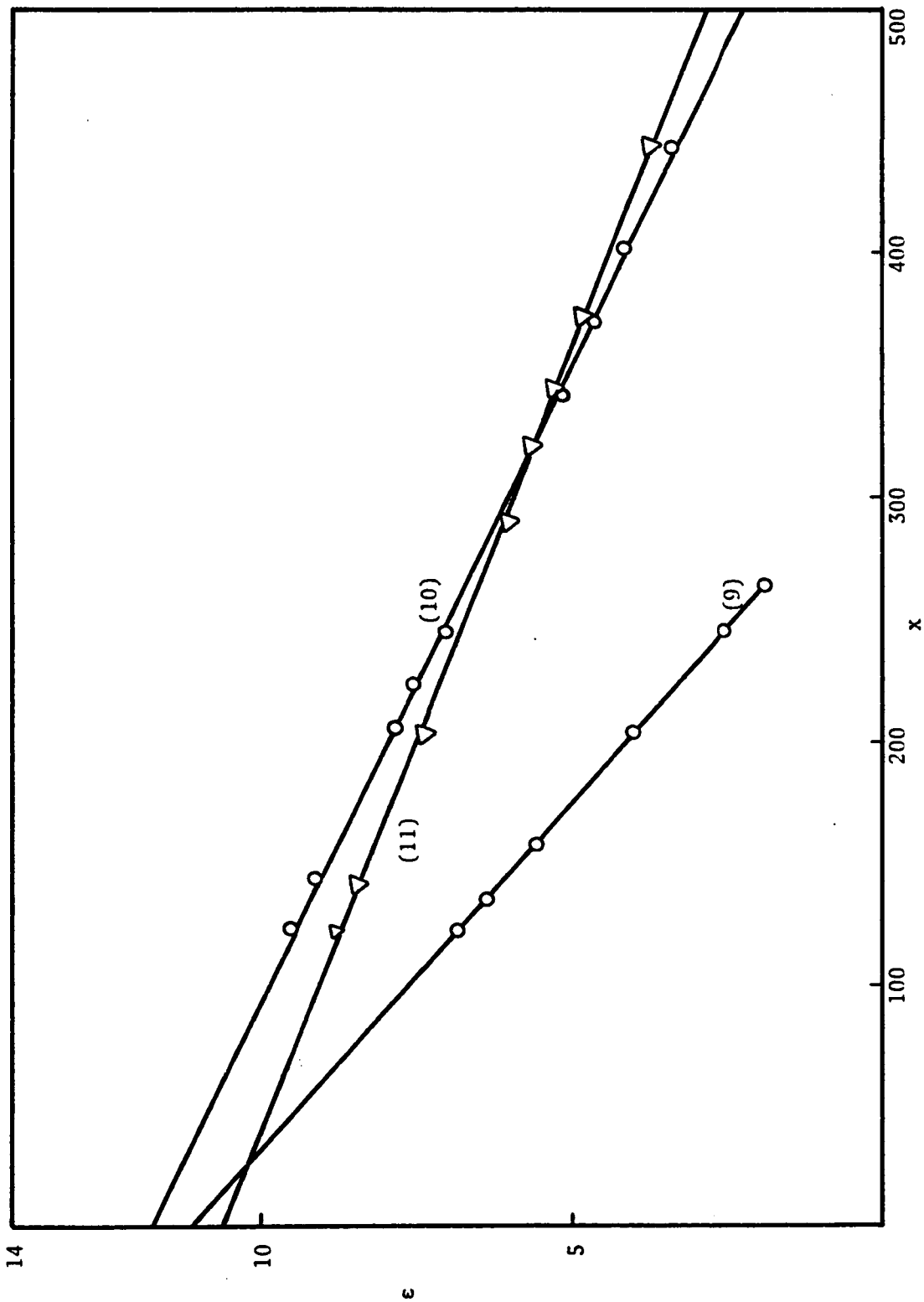

Figure (V-8): Typical graphs of ε vs. λ^2 for $Ga_{1-x}Al_xAs$ alloys.

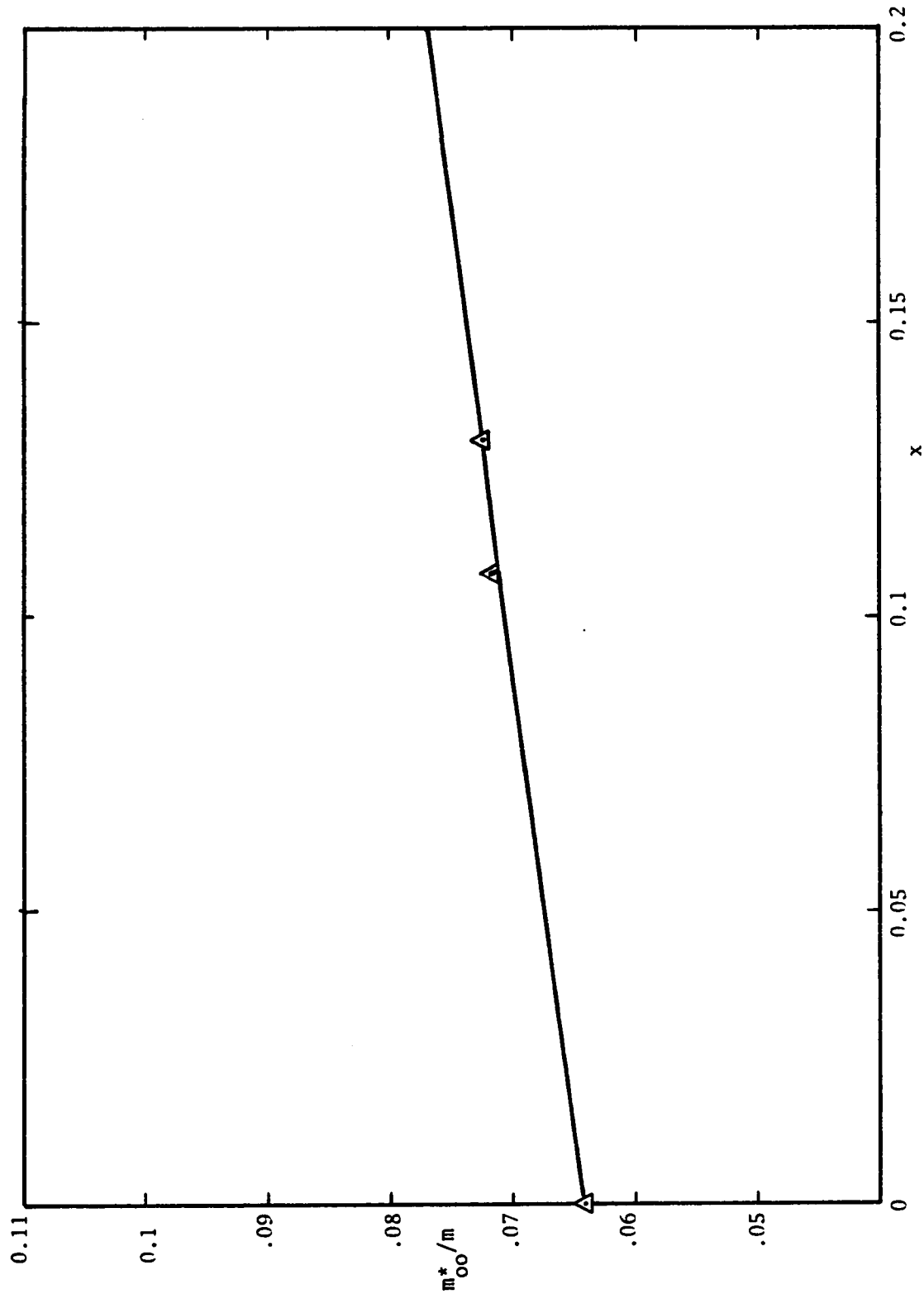

Figure (V-9): Variation of m^*_{oo}/m with composition for $Ga_{1-x}Al_xAs$ alloys.

APPENDIX

COMPUTER PROGRAMME

```
               C
               C
               C
               C
               C
               C
               C
               C
               C
               C
               C
               C      PROGRMN TO CALCULATE THE EFFECTIVE MASS OF THE BOTTOM OF THE(000)
               C      BAND IN THE GENERAL DEGENEZCY CASE BY THE SIMULTANEOUS SOLUTION OF
               C      THE INTEGRAL GIVING THE FREE CARRIER REFLECTIVITY AND CARRIER'
               C      CONCENTRATION INTEGRAL
               C      ARE CALCULATION AS A FUNCTION OF THE FERMI LAVE
               C      ALL UNITS ARE M.K.S.
               C
               C
0001                  DIMENSION CO(80),EF(80),EFMO(80),CONC(80),FEMO(80),EGS(80),
                     &XEMO(80),SLOPE(80),AI1(80),AI2(80)
0002                  READ(5,49) NSPE,NMO
0003              49  FORMAT(2I3)
0004                  READ(5,40)(CO(K),SLOPE(K),CONC(K),EGS(K),EF(K),K=1,NSPE)
0005              40  FORMAT(5E15.3)
0006                  READ(5,44) (EFMO(L),L=1,NMO)
0007              44  FORMAT(10F8.4)
0008                  DO 125 L=1,NMO
0009             125  FEMO(L)=((1.0/EFMO(L))-1.00)
0010                  AKT=0.02550
0011                  ALPHA=3.8098E-20
0012                  K=1
0013             105  DO 511 L=1,NMO
0014             511  XEMO(L)=EGS(K)*FEMO(L)
0015                  L=1
0016                  M=1
0017                  N=1
0018                  DELE=1.0E-03
0019                  WRITE(6,43) EF(K),EGS(K),SLOPE(K)
0020              43  FORMAT(1H1, 14HFERMI ENERGY =,F7.4,10X,21HADJUSTED ENERGY GAP =,F6
                     &.4,7HSLOPE =,E15.6/)
0021                  WRITE(6,42)
0022              42  FORMAT(1H0,2X,10HCMPOSITION,24X,15HEFFECTIVE MASS ,5X,12HCARRIERCO
                     &NC ,5X,15HEFFECTIVE MASS//)
0023                  WRITE(6,41)
0024              41  FORMAT(1H ,4X,9H(PERCENT),23X,17HAT BOTTOM OF BAND,3X,14H(PER METE
                     &R**3),7X,10HCALCULATED//)
0025             102  EVEN1=0.000
0026                  EVEN2=0.00
0027                  ODD2=0.00
0028                  ODD1=0.000
0029                  AEE=EF(K)-5.0E-01
0030                  IF(AEE.LT.0.0)AEE=0.0
0031                  AEO=AEE+5.0E-04
0032                  DO 100 J=1,500
```

```
0033                  ENE=(AEE*(AEE+EGS(K)))
0034                  ENO=(AEO*(AEO+EGS(K)))
0035                  SE=(AEE-EF(K))/AKT
0036                  SO=(AEO-EF(K))/AKT
0037                  TE=EXP(SE)
0038                  TO=EXP(SO)
0039                  UF=1.00/TE
0040                  UO=1.00/TO
0041                  HE=2.0+TE+UF
0042                  HO=2.0+TO+UO
0043                  IF(N-1) 106,106,107
0044             106  RIE=(1+(EFMO(L))/((1+4*ENE/(EGS(K)**2))**0.5))
0045                  RIO=(1+(EFMO(L))/((1+4*ENO/(EGS(K)**2))**0.5))
0046                  FIE=((ENE**1.5)*(RIE))/HE
0047                  FIO=((ENO**1.5)*(RIO))/HO
0048                  EVEN1=EVEN1+FIE
0049                  ODD1=ODD1+FIO
0050             107  IF(N-1) 108,108,109
0051             108  F2E=(ENE**1.5)/HE
0052                  F2O=(ENO**1.5)/HO
0053                  EVEN2=EVEN2+F2E
0054                  ODD2=ODD2+F2O
0055             109  AEE=AEE+DELE
0056             100  AEO=AEO+DELE
0057                  IF(N-2) 117,118,118
0058             117  AI1(L)=(DELE/6.0)*(4.0*EVEN1+2.0*ODD1)*(7.93871E+02)
                    &/((AKT*ALPHA**0.5)*XEMO(L)**1.5)
0059                  IF(AI1(L)-SLOPE(K))110,111,111
0060             111  N=2
0061                  IF(L-2) 118,116,116
0062             110  CONTINUE
0063             118  IF(N-2) 115,124,124
0064             115  AI2(L)=(DELE/6.0)*(4.0*EVEN2+2.0*ODD2)*3.3774E-02/((ALPHA**1.5)*
                    &AKT*XEMO(L)**1.5)
0065                  IF(AI2(L)-CONC(K)) 500,112,112
0066             112  N=2
0067                  GO TO 119
0068             500  WRITE(6,50) CO(K),EFMO(L),AI2(L),AI1(L)
0069              50  FORMAT(1X,E12.4,27X,E12.4,5X,E12.4,8X,E12.4)
0070                  IF(L-NMO)120,101,101
0071             120  L=L+1
0072                  GO TO 102
0073             114  SLOTG=(EFMO(L)+(AI1(L)-SLOPE(K))*(EFMO(L)-EFMO(L-1))/(AI1(L-1)-
                    &AI1(L)))
0074                  GO TO 113
0075             119  CONTG=(EFMO(L)+(AI2(L)-CONC(L))*(EFMO(L)-EFMO(L-1))/(AI2(L-1)-
                    &AI2(L)))
```

```
0076              GO TO 500
0077          124 IF(M-2) 500,122,122
0078          122 WRITE(6,121)SINIG,CNIG
0079          121 FORMAT(3X,42HEFFECTIVE MASS FOR EFFCTIVE MASS INTEGRAL =,F12.4,
                 &10X,39HEFFECTIVE MASS FOR CARRIER CONCENTION =,E12.4//)
0080          101 IF(K-NSPE)103,104,104
0081          103 K=K+1
0082              GO TO 105
0083          104 STOP
0084              END
```

REFERENCES

F1 Faraday, M. Expt. Res. in Elec. Series 4, 433(1833)

B1 Braun, F. Ann. Phys. Chem. 153, 566(1874)

S1 Smith, W., J. Soc. Tel. Engr., 2, 31 (1873)

H1 Hall, E. H. Am. J. Math., 2, 287(1879)

B2 Bardeen, J. and Brattain, W. H., Phys. Rev. 75 1208(1949)

28L Langmuir, I. Proc. Nat. Acad. Sci. Wash. 14 627 (1928).

51B Bohm and Pines, D. Phys. Rev. 82, 625(1951).

52P Pine, D. Phys. Rev. 85, 338(1952)

52W Welker, H. Z. Naturforsch, 70, 744(1952)

53B Bohm and Pines, D. Phys. Rev. 85, 338(1953)

53D Downie, A. R., Magoon, M. C., Thomasine, P. and Crawford, B. Jour. of Optical Society of American, 53, 941(1953)

53P Pine, D. Phys. Rev. 92, 629(1953)

55B Bohm and Pines, D. Phys. Rev. 92, 609(1955)

55P Parmenter, R. H. Phys. Rev. 97, 587(1955)

57E Ehrenreich, H., J. Phys. Chem. Solid 2, 131(1957)

57K Kane, E. J. Phys. Chem. Solids 1, 249(1957)

57L Larach, S., Schrader, R. E. and Stocker, C. F. Phys. Rev., 108, 587(1957)

58V van der Pauw, L. J. Philips Res. Repts. 13, 1(1958)

58

59S Smith, R. A., "Semiconductors" Cambridge (1959)

59S1 Spitzer, G. and Whelan, J. M. Phys. Rev. 114, 59(1959)

60L Lax, B. and Mavroides, J. G. Solid State Phys. 11, 161(1960).

62B Bennett, H. B., Bennett, J. M., and Ashley, E. J. Jour. of the Optical Society of American 52, 1245(1962)

62K Kolodziejczak, Acta. Phys. Polon. 21, 637(1962).

62W Wlopzimterz, Zawadzki. Physica Stat. Sol. 2, 385(1962)

62Z Zawadzki, Phys. Stat. Sol. 2, 385(1962)

63A Allen, J. W. and Hodby, J. W., Proc. Phys. Soc. 82, 315(1963)

63C Cardona, M. Phys. Rev. 129, 69(1963)

63Z Zawadzki, W., Phys. Stat. Sol. 3, 990(1963)

64K Kittel, K., "Quantum Theory of Solids" John Wiley and Sons, 224(1964).

64L Lyden, H. Phys. Rev. 134, A1106(1964)

64M Madelung, O. and Meyerhofer, D. "Physics of III-V compounds" John Wiley and Sons, 31(1964)

64S Spitzer, W. G. and Mead, C. A. Phys. Rev. 173(1964)

66KA Kane, E. O., "In Semiconductors and Semimetals 1" (Willardson, R.R., Beer, A.C., eds.) Academic Press, New York 75(1966).

67Th Thompson, A. G. and Woolley, J. C. Can. J. Phys. 45, 255(1967).

67B Bruamstein, R. and Kane, E. O. J. Phys. Chem. Solids, 23, 1423(1967).

69B Blom, F. A. P. and Schrama, J. Th. Phys. Letters, 30A, 245(1969).

69S Stukel, D. J. and Euwema, R. N., Phys. Rev. 188, 1193(1969)

69T Thomas, B. M. Ph.D. Thesis, Department of Physics, University of Ottawa, (1969)

69V Van Tongerloo, E.H. and Woolley, J. C. Can. J. of Phys. 47, 241(1969)

70A Antypas, G. A., James, L. W., and Uebbing, J. J. J. Appl. Phys. 41, 2888(1970)

70B Bergstresser, T. K. and Van Vechten, J. A. Phys. Rev. 1, 335(1970)

70C Cahn, R. N. and Cohen, M. L. Phys. Rev. B. 1, 2569(1970)

70H Hwang, J. Appl. Phys. 41 2668(1970)

70S1 Stroud, D., Ehrenreich, H., Phys. Rev. B2, 3197(1970).

70T Thomas, M. B., Coderre, W. M. and Woolley, J. C. Phys. Status Solidi A2, k141(1970).

70TA) Taylor, A. and Fortin, E. Can. J. Phys. 48, 1874(1970).

71R1) Richardson, J. Phys. C4 L 289(1971)

71W Berolo, O. and Woolley, J. Can. J. Phys. 49, 1335(1971)

72B Bestide, G., Pistoulet, B., Robert,J. L. and Roustan, C. Solid State Com. 11, 835(1972)

72C Cohne, M. M. "Introduction to Quantum Theory of Semiconductors" Gordon and Breach Publ. 152(1972).

72D Dionne, G. Ph.D. Thesis, Department of Physics, University of Ottawa (1971).

72R Rosenbaum, S., Ph.D. Thesis, Department of Physics, University of Ottawa (1972)

72R1 Richard, J. Stirn "Semiconductors and Semimetals" by W. Beer, vol. 8, 55(1972).

72R2 Richardson, J. Phys. C5 L27(1972)

72W Berolo, O., Van Vechten, J., and Woolley, J. C. Phys. Rev. Lett. 29, 1400(1972).

72Z Ziman, J. M. "Principles of the Theory of Solids", Cambridge Publishers, 185(1972)

73G Gratton, M. F. and Woolley, J. C. J. of Electrochem. Materials. 2, 455(1973)

73H Hess, E. J., Topol, K. R., Schulze, H. and Uncer, K. Phys. State. Sol. (b) 55, 187(1973)

73M Monemar, B. Phys. Rev. B8, 5711(1973).

73S Song, K. S. Solid State Commun. 13 1397(1973)

73W Woolley, J. C., Berolo, O. and Van Vechten, J.A. Phys. Rev. B. 8, 3794(1973).

73Y Yanezawa, F., Morigaki, K. Prog. Theor. Phys. Suppl. 53, 1(1973)

74A Antypas, and Moon, R. L. J. Electrochem. Soc. 121, 416(1974).

74C Chwang, R. B. Smith, J. and Crowell, C. R. Solid State Electronic, 17, 1217(1974).

74E Elliott, R. J., Krumhansal, J. A., and Leath, P. L. Rev. Mod. Phys. 46, 565(1974).

74F Filion, A. and Fortin, E. Can. J. Phys. 52, 743(1974).

74K Kukharskii, A. A. and Ryzhkova, E. A. Sov. Phys. Semicon. 7, 876(1974).

74H Hill, and Pitt, . J. Phys. C7, 521(1974).

74S1 Siggia, E. D. Phys. Rev., B10, 5147(1974).

74S1 Springthorpe, A. J., King, F. D. and Becke, A. J. of Electronic Materials, 4, 101(1975).

74RO Rode, D. L. J. of Appl. Phys. 45, 3887(1974).

74R Radautsan, E. k., Arushanov, and Nateprov, A. N. Phys. Solid State (a) 23, K59(1974).

75A Arushanov, E. K., Nateprov, A. N. and Chuiko, G. P. Sov. Phys. Semicond. 8, 14(1970).

75B Basinski, J. and Woolley, J. C. J. Phys. C.: Solid State Phys. 8, 1841(1975).

75K1 Kozo Osamura and Votaro Murakami, J. Phys. Chem. Solid 36, 931(1975).

75K Kumar, V. D., Kumar, S. K. Joshi. Phys. Rev. B11, 283(1975)

75N1 Nahory, and Pollack, Appl. Phys. Letters, 27, 562(1975).

75R Rosenbaum and Woolley. Can. J. Phys. 53, 1071(1975)

76D Devlin, Paul, M.Sc. Thesis, Department of Physics, University of Ottawa, p. 65(1976).

76AS Aspnes, D. E. Physical Review, B, 14, 5331(1976)

76N Naruo Nagui and Yoshio Noguchi. J. Applied Phys. 47, 5484(1974).

77C Czachora, Acta. Phys. A51, 283(1977)

77C1 Cho, A. Y., Carey, H. C. and Foy, P. W. Appl. Phys. Letters, 30 (1977).

77T Tripathi, , and Moseley, L. L. Solid State Comm. 21, 655(1977)

77N1 Nahory, R. E., Pollack, M. A. Dewinter, J. C. and Williams, R. M. J. of Appl. Phys. 48, 1607(1977).